UNIVERSITEIT GENT

FACULTY OF SCIENCES

Towards structure-function studies of Myristoyl-CoA:Protein N-myristoyltransferase from the malaria parasite *Plasmodium falciparum*

TA DUY TIEN

Master's dissertation submitted to obtain the degree of
Master of Biochemistry and Biotechnology
Major Biochemistry and Structural Biology
Academic year 2008-2010

Promoter: Prof. Dr. Savvas Savvides
Scientific supervisor: Kedar Moharana
Department of Biochemistry and Microbiology
Laboratory for Protein Biochemistry & Biomolecular Engineering

L-ProBE

Acknowledgments

First and foremost, I would like to give a big thank to my supervisor, Mr. Kedar Moharana, for all of your supports for my project. I strongly appreciate your scientific guidance and advices, and especially your careful revision for my thesis. Moreover, your enthusiasm in research has made a deep impression on my mind, and made me feel very motivated in biological science also.

I am very thankful to my promotor, Professor Savvas Savvides, the group leader of the L-ProBE lab (Laboratory for Protein Biochemistry and Biomolecular Engineering, Universiteit Gent), for offering the project on malaria parasite Plasmodium falciparum NMT. Your strong inspiration in structural biology has, indeed, directed my research interest into the field and has been a strong motivation for me to come to this project.

The next big thank I would like to say is to all other members in the L-ProBE lab, who did help me a lot to get familiar with such a hard lab working at the beginning, and also during the time I was there. Thank Bjorn for giving me very helpful advices in protein purification. Thank Lina, Isabel, Ester, and Annelies for explaining the lab facilities usage to me. Thank Kenneth for giving me your thrombin stock for the His-tag digestion experiment. Thank Ann, Géraldine, Jonathan, Ruben, and Nathalie for helping me to solve my problems regarding the practical work. And lastly, I would like to thank Freddy for your effort on washing, cleaning, and sterilizing all the laboratorial stuffs; without you, I could not finish my project for sure.

My special thank and acknowledgment to The Mekong 1000 – Can Tho 150 Project, which offered a financial support for my master program. In fact, I have had two wonderful years in Belgium for studying new tremendous knowledge, and also had a chance to reach and understand many different cultures in Europe. I would like to honestly say ‘thank’ to Professor Ann Depicker and Dr. Hilde Nelissen, who helped me a lot in my application so that I could follow the Biochemistry and Biotechnology master program at Universiteit Gent.

I cannot forget to thank all my friends, who are my strong supports in several ways so that I could get along with my thesis to the end. Thank all my classmates, especially Ellen, Jan, Klass, Mariska, Nienke, who also worked in L-ProBE lab for their theses. You could explained my doubts immediately and give me some useful hints, especially on the Western blotting. Sometimes you kindly gave me your prepared SDS-PAGE gels when I urgently needed them. Thank all my Vietnamese friends in Gent and in my home country: Huy, Trân, Vân, Triều, Hạnh, Khương, Việt Anh, Ninh, Phong, etc. You are my big mental support. I can never forget the time of parties and journeys we had together. You guys really made me feel a feeling of family here in Gent, without which I would definitely have given it up soon. Also thank my friends: Phát, Hùng, Hồ, Nguyên, Pháp who kindly sent me valuable documents for reference.

Last but not least, I would like give my thank to my Grandma, Dad, Mom, and my Little Sister. Thank you for your everlasting love for me. I love all of you.

June 2010

Ta Duy Tien

Table of contents

List of Abbreviations

2xYT	two times yeast extract-tryptone medium
AK2	Adenylate kinase 2
ARF	ADP-ribosylation factor 1
BSA	Bovine Serum Albumin
*Ca*NMT	*Candida albicans* N-myristoyltransferase
CoA	Coenzyme A
Dsrc42A, Dsrc64B	*Drosophila* non-receptor tyrosine kinases
FPLC	Fast Protein Liquid chromatography
GNAT	GCN5-related *N*-acetyltransferase>
HEPES	4-(2-hydroxyethyl)-1-piperazineethanesulfonic acid
His-*Pf*NMT	N-myristoyltransferase with 6xHis tag at N-terminus
HIV	Human Immunodeficiency Virus
IEX	Ion exchange chromatography
IMAC	Immobilozed metal affinity chromatography
IPTG	Isopropyl b-D-1-thiogalactopyranoside
LB	Lysogeny broth or Luria-Bertani broth
MARCKS	Myristoylated alanine-rich C kinase substrate
MCoA	Myristoyl-Coenzyme A
MES	2-(N-Morpholino)ethanesulfonic acid
NMT	N-myristoyltransferase
Nmt1p	Saccharomyces cerevisiae N-myristoyltransferase
OD_{600}	Absorbance at 600 nm
ORF	Open-reading frame
$p60^{src}$	Tyrosine kinase of *Rous sarcoma* virus with MW of 60,000
PBS	Phosphate buffer saline
PIP_2	Phosphatidylinositol bisphosphate
*Pf*AK2	*Plasmodium falciparum* adenylate kinase 2
*Pf*NMT	*Plasmodium falciparum* N-myristoyltransferase
rpm	rounds per minute
*Sc*NMT	*Saccharomyces cerevisiae* N-myristoyltransferase
SDS	Sodium dodecyl sulfate
SDS-PAGE	Sodium dodecyl sulfate polyacrylamide gel eclectrophoresis
SEC	Size exclusion chromatography
SPA	Scintillation proximity assay
TB	Terrific broth
*Tb*NMT	*Trypanosoma brucei* N-myristoyltransferase
Tris	Tris(hydroxymethyl)aminomethane
UNICEF	United Nations Children's Fund
v/v	Volume per volume
w/v	Weight per volume
WHO	World Health Organisation

List of Tables

List of Figures

Summary

Millions of deaths per year because of malaria make it become one of the most dangerous infectious diseases in tropical and subtropical regions. The disease is caused by the parasitic protozoan of the genus *Plasmodium*, among which *P. falciparum* is the most severe and fatal. The parasites are transmitted to human by female *Anopheles* mosquitoes. The *Plasmodium* parasites have a complex life cycle comprising multiple stages with the alternation between asexual and sexual production in both mosquito and human hosts. Recently, the development of anti-malarial drugs is a big challenge due to the difference in the susceptibility and sensitivity of each life form of the parasite, as well as the very fast increase of drug resistance.

Protein:Myristoyl-CoA N-myristoyltransferase (briefly NMT) from *P. falciparum* has been identified as a promising anti-malarial target. The enzyme catalyzes the transfer of myristate, a fourteen-carbon fatty acid, to the N-terminal glycine of the target protein or peptide. NMT is an essential enzyme in several organisms, especially the pathogens such as *Candida albicans*, *Trypanosoma brucei*. A putative substrate for NMT in *P. falciparum* was identified as adenylate kinase 2 (AK2). Besides, there is very little information about the structure and function of the enzyme that has been reported.

In this study, the gene coding for *P. falciparum* NMT (*Pf*NMT) was cloned into *Escherichia coli* with a N-terminal 6xHis tag for over-expression. The recombinant protein (designated as His-*Pf*NMT) was purified using several chromatographic techniques including immobilized metal affinity chromatography (IMAC), ion exchange chromatography (IEX) and size exclusion chromatography (SEC). The total yield was approximately 100 μg per liter of *E. coli* culture. The purified His-*Pf*NMT underwent crystallization trial for structure solving by X-ray crystallography. The crystallization screen was set up with fifty-five conditions with protein concentration varying from 8.8 $mg.ml^{-1}$ to 18 $mg.ml^{-1}$ but no hit has been achieved yet.

In vitro enzymatic assay with myristoyl-Coenzyme A and synthetic octapeptide substrate (derived from N-terminal sequence of AK2) indicated that His-*Pf*NMT was more active, and probably more stable, at slightly acidic pH. The optimal temperature for the enzyme activity was determined as 37^0C, with is physiological temperature of human body. The Michaelis-Menten constants (K_m) of His-*Pf*NMT and *Pf*NMT without the 6xHis-tag for the octapeptide were experimentally calculated as 551.4 and 692.6 μM, respectively.

Part 1: Introduction

1.1. Malaria

1.1.1 What is malaria?

Malaria is a parasitic infectious disease, which affects approximately 500 million people and causes 2 million deaths each year. It occurs mostly in tropical and subtropical regions where nearly 3 billion people are living. Malaria distribution and endemicity is showed in Figure 1 (Malaria and Children, 2007).

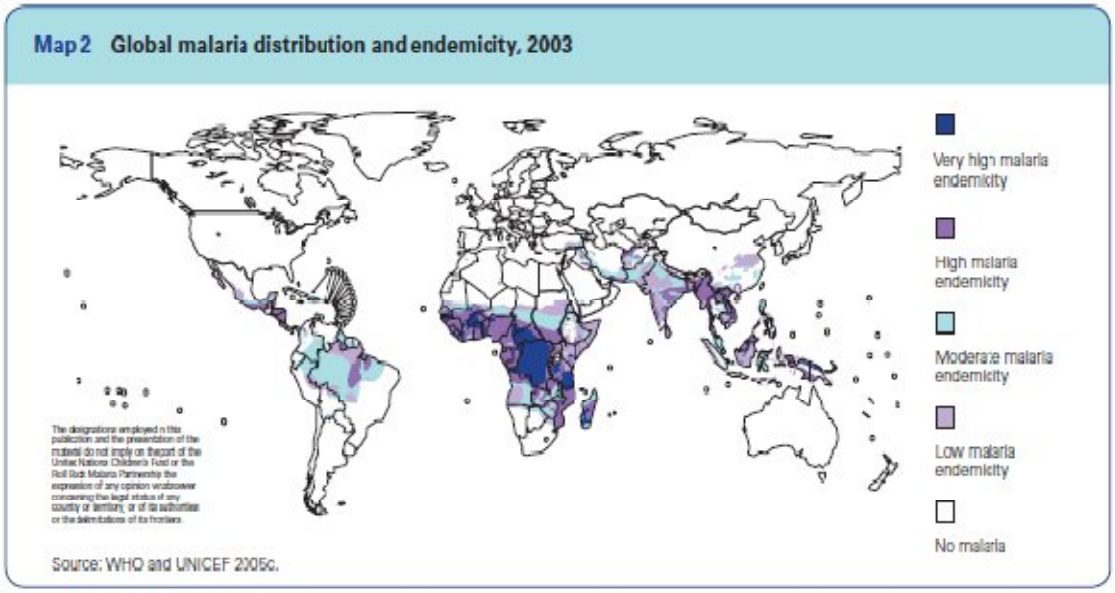

Figure 1: Global distribution and endemicity of malaria (Malaria and Children, 2007)

Malaria is one of the leading killers of children under five years old, and is accounting for almost one death in ten cases worldwide. It has been also reported from clinical studies that there is a strong interaction between HIV and malaria since it is one of the opportunistic infection with highest risk for HIV/AIDS patients, who suffer from immunity failure. The efficacy of malaria treatment might be also reduced in these infectious patients. Pregnant women are particularly vulnerable because evidence shows that HIV lessens pregnancy-specific. In other studies, malaria potentially impacts the progression and transmission of HIV since it might increase the viral load in HIV-positive patients (Wahlgren, M. and Perlmann, P., 2005).

1.1.2 Malaria parasites

Malaria is caused by the protozoan parasites of the genus *Plasmodium* (Figure 2) that are transmitted by infected female *Anopheles* mosquitoes. The parasites enter the human bloodstream through the mosquito bite, which mostly occurs at night.

The genus *Plasmodium* was coined in 1885 by Marchiafava and Celli. Currently over 200 species are recognized (Perkins and Austin 2009). New species continue to be described. However, only four of them cause human malaria: *Plasmodium falciparum*, *Plasmodium malariae*, *Plasmodium ovale*, and *Plasmodium vivax*, among which *P. falciparum* is the most common and deadly. Other species infect other animals, including birds, reptiles and rodents. The parasite always has two hosts in its life cycle: a mosquito vector and a vertebrate host (Goodman, Gilman et al. 2008).

Domain: Eukaryota
Superphylum: Alveolata
Phylum: Apicomplexa
Class: Aconoidasida
Order: Haemosporida
Family: Plasmodiidae
Genus: ***Plasmodium***

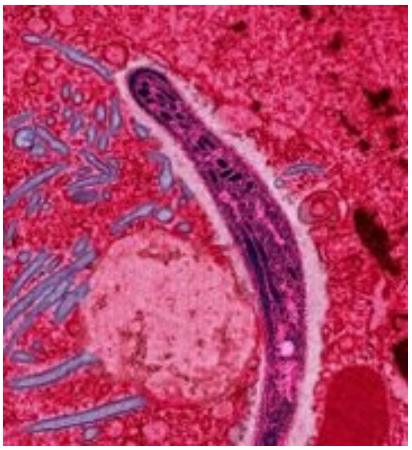

Figure 2: Classification of the genus *Plasmodium* (left) and a malaria parasite in a vertebrate cell (right) (image from http://en.wikipedia.com/Plasmodium)

1.1.3 A complex life cycle

The *Plasmodium* is a single cell organism possessing a complex life cycle with the alternation of asexual and sexual reproduction stages (Figure 3) (Marcus 2009). This means an asexually-reproducing generation (cell division by mitosis) alternates with a generation in which the parasites form sex cells, precede cell fusion to produce offspring with the recombination of genetic materials and appearance of new traits.

Asexual stage

Infected mosquitoes, carrying parasitic sporal form called sporozoites in the salivary glands, bite and transmit them to human. When in the bloodstream, the sporozoites immediately head to the liver and completely penetrate to the organ very fast (within 30 minutes to one hour). Inside the hepatocytes, the parasites continuously multiply through mitosis and develop into tissue schizonts for 9 to 16 days. After this stage, tissue schizonts rupture and release a new form of the parasites called merozoites, followed by their invasion into erythrocytes to initiate the erythrocytic cycle in which they feed on hemoglobin and continue their asexual division (Marcus 2009).

After a few asexual reproductive cycles, the maturation of all of the parasites becomes more or less coordinated, and the blood cells begin to rupture quite simultaneously. The parasites are then released and quickly infect new cells, and repeat the above cycles for several times (Marcus 2009).

Sexual stage

Eventually, the asexual stage of the parasite life cycle comes to an end. Most of them re-invade the liver and remain in the organ for a long time, whistle some cells emerge as gametocytes. These gametes are occasionally picked up by female Anopheles mosquitoes through biting the malaria carriers, and then undergo the sexual fertilization to form diploid zygotes. Later on, the resulting zygotes develop to oocysts in the mosquitoes gut and finally give rise to sporozoites, which invade the salivary gland of the mosquitoes (Marcus 2009).

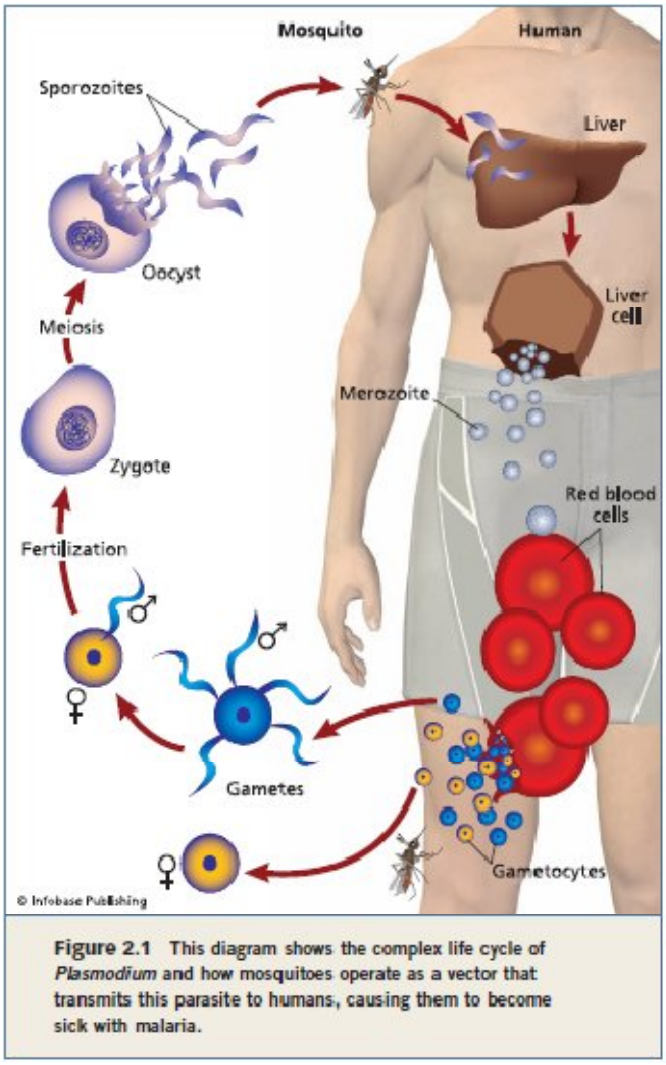

Figure 3: The complex cell cycle of *Plasmodium* (Marcus 2009)

1.1.4 Anti-malarial drugs

The complex life cycle of the malaria parasites with multiple stages results in the difference in drug sensitivity of each stage (Goodman, Gilman et al. 2008). Thus, the anti-malarial drugs are best classified in the context of the parasite life cycle.

There has been no effective drug against the sporozoites infection at this moment; therefore the main target is to prevent the development of symptomatic malaria

caused by the asexual erythrocytic forms. Moreover, none of the anti-malarials is effective against all liver and red cell stages of the life cycle that might coexist in a patient. Complete cure therefore may require more than one drug.

Some well-known anti-malarial drugs such as Chloroquine, Quinine, Sulfadoxine. Artemisinins are reported as potential anti-malarials with no clinical evidence of resistance. For that reason, they are promising for treatment of the most lethal malaria caused by *P. falciparum*. These drugs, however, have not been approved by FDA yet, and inactive counterfeits are common. Recently, the low efficacy of therapeutic drugs is mostly due to quickly increasing drug resistance by parasites (Goodman, Gilman et al. 2008).

1.2. N-Myristoylation

1.2.1 What is 'N-Myristoylation'

'N-Myristoylation' refers to the covalent attachment of myristate, a 14-carbon saturated fatty acid, to the N-terminal glycine of target peptides/proteins. This is a post-translational and irreversible modification in eukaryotic organisms (Farazi, Waksman et al. 2001). It may also occur co-translationally following the removal of the initiator methionine residue by cellular methionyl-aminopeptidases. Pathogenic viruses and bacteria usually lack the enzymes needed for this modification, and thus this kind of modification is carried out by the host enzymes (Maurer-Stroh and Eisenhaber 2004).

1.2.2 Targets of 'N-Myristoylation'

A wide range of protein family has been reported to undergo myristoylation, including cAMP-dependent serine/threonine kinases, retroviral polyprotein precursors such as HIV-1pr55, viral capsid components, and the α-subunit of many signal-transducing, heteromeric G proteins. Some of these are cytosolic, whilst most proteins are associated with cellular membrane since the overall hydrophobicity of the N-termini is greatly enhanced by the long acyl chain of myristoyl, permitting a better association with the membrane lipid bilayer (Price, Menon et al. 2003).

1.2.3 Biological functions of 'N-Myristoylation'

The addition of myristoyl group to the newly synthesized proteins has diverse functions and intracellular destinations to promote weak and reversible protein-membrane and protein-protein interactions, or trigger transduction cascades (Farazi, Waksman et al. 2001). Typically, myristate moiety acts in concert with other mechanisms to regulate protein targeting and functioning. Some proteins, for example MARCKS protein in budding yeast employ "myristoyl-electrostatic switches" where membrane association is promoted by myristate plus electrostatic interactions between positively charged protein side chains and negatively charged membrane phospholipids (Farazi, Waksman et al. 2001).

Other *N*-myristoylated proteins like ARF1 (ADP-ribosylation factor 1), recoverin or proteolytic cleavage (HIV-1 Pr55gag/p17MA) produces a conformational change that exposes or sequesters the acyl chain ("myristoyl-conformational switch"). A subset of proteins may undergo post-translational covalent modification with one or more palmitoyl groups after N-myristoylation. The limited hydrophobicity of the myristoyl anchor permits reversible membrane interactions and requires additional membrane attachment factors (MAFs) for enhancing membrane targeting. Typical MAFs include the subsequent palmitoylation of the cysteine residues nearby, clusters of positive charges, phospholipid-binding domains (e.g. for PIP_2 interactions), transmembrane regions or direct protein–protein interactions. Both targeting specificity and membrane affinity are achieved through the concerted effects of a combination of these MAFs. For example, dual acylation (myristoylation and palmitoylation) often directs proteins to lipid rafts. In viruses in particular, the role of the myristoyl moiety includes not only targeting to diverse membranes and membrane sub-compartments, but it can also be involved in direct interactions with other proteins or conformational switches that affect tertiary and quaternary structure (Maurer-Stroh and Eisenhaber 2004). Furthermore, reports also suggest that acylation at specific locations has an impact on the secondary or tertiary structure of the protein, particularly induced-folding of such as, recoverin and transducin. Myristoylation in conjunction with other events (Ca^{2+} binding or phosphorylation) can also induce conformational changes (Boutin 1997).

Two of the most thoroughly studied myristoylated proteins are the transforming protein of *Rous sarcoma* virus, $p60^{v\text{-}src}$, and the proto-oncogene product, $p60^{c\text{-}src.}$ These polypeptides are translated on free polysomes and myristoylated before being transported to the plasma membrane. Deletion or modification of the first 14 N-terminal amino acids of $p60^{c\text{-}src}$ does not influence its intrinsic tyrosine kinase activity, but prevents myristoylation and membrane association, and thus abolishes the transforming activity of the protein. Together, these observations suggest an important role of myristylation in targeting proteins to the plasma membrane and in cellular transformation (Wilcox, Hu et al. 1987)

1.3. Myristoyl-CoA:Protein N-Myristoyl transferase

N-Myristoylation is catalyzed by myristoyl-CoA:protein *N*–myristoyl transferase (NMT) (EC 2.3.1.97), a member of the GNAT (GCN5-related *N*-acetyltransferase) superfamily. Nineteen NMTs have been identified from 15 species. The *Saccharomyces cerevisiae* genome contains a single *NMT* gene. *Arabidopsis thaliana* contains two *NMT* genes. Three mammalian species (human, mouse, bovine) each possess two NMTs (termed type I and type II). *Saccharomyces cerevisiae* NMT (Nmt1p) is the first one to be isolated (Towler, Adams et al. 1987) and since then the enzyme has been identified and characterized in many other organisms including fungi (*Candida albicans*, *Cryptococcus neoformans* (Wiegand, Carr et al. 1992; Lodge, Johnson et al. 1994)), parasitic protozoa (*Leishmania major*, *Trypanosoma brucei*, *Plasmodium falciparum*) (Gunaratne, Sajid et al. 2000; Price, Menon et al. 2003)) and mammals (*Homo sapiens* (Duronio, Reed et al. 1992)). About 0.5 % - 1.7% of the proteome may undergo *N*-myristoylation depending on the organism

(Maurer-Stroh, Eisenhaber et al. 2002; Boisson, Giglione et al. 2003; Boisson and Meinnel 2003).

In mammals, both type I and type II NMTs show a high degree of conservation across species. Type I and II NMTs are most divergent at their N-termini (Glover, Hartman et al. 1997). The extended N-terminal domain of type I human NMT may be involved in targeting the enzyme to the ribosome but is not required for activity *in vitro*. The divergent N-terminal domains of the two NMT isoforms may be responsible for differential cellular localization, thereby effecting co-translational ribosome-based or post-translational cytosol-based acylation of the proteins (Glover, Hartman et al. 1997; Farazi, Waksman et al. 2001).

1.3.1 NMT is an essential enzyme

The *Saccharomyces cerevisiae* genome contains a single *NMT* gene. Over-expression of this gene by means of the yeast episomal plasmid YEp24 showed no obvious effects on growth kinetics or cell morphology. Insertional mutagenesis of the *Nmt1p* locus on yeast chromosome XII, however, caused recessive lethality, indicating that this enzyme is necessary for yeast vegetative cell growth (Duronio, Towler et al. 1989).

An *NMT* null allele also causes lethality in the two major causes of systemic fungal infections in humans: *Candida albicans* and *Cryptococcus neoformans* (Farazi, Waksman et al. 2001). NMT has also been reported to be essential in other kinetoplastid protozoan parasites such as *Trypanosoma brucei* (Price, Menon et al. 2003). Down-regulation of *TbNMT* gene by RNAi technique resulted in parasites population with aberrant morphology such as rounded or abnormally elongated cells, carrying more than one flagellum and displaying partial plasma membrane detachment. High cell death rate was observed in both procyclic and bloodstream stage of *T.brucei*.

NMT role in plants has not been clearly elucidated yet. Studies on *Arabidopsis thaliana* revealed two NMT genes, one of which, namely *AtNMT1*, was firstly described in higher plants. *AtNMT1* was strongly expressed in young, developmentally active tissues such as root, leaf (15 days after planting), flowers, and its function was highly associated with ribosomal fraction in leaf extract (~60% enzymatic activity). Transgenic lines generated by antisense suppression of *AtNMT1* displayed significant growth reduction, fewer rosette leaves, shortened life-span and inability to produce seeds (Qi, Rajala et al. 2000).

A null mutation of *Drosophila melanogaster* results in embryonic lethality (Ntwasa, Aapies et al. 2001). Mutant embryos display a range of phenotypes, including morphogenetic abnormalities associated with disordered cell movement and widespread apoptosis. Some of these changes produced by genetic manipulations affect *D. melanogaster* N-myristoylated proteins, which are involved in dynamic rearrangements of the actin cytoskeleton, e.g. non-receptor tyrosine kinases (Dsrc42A, Dsrc64B).

In mice, although the two isoforms of NMT are very similar in structure and peptide specificity, they function differently. Nmt1 is the principal *N*-myristoyl transferase in early embryogenesis, and is required for normal development (Yang, Shrivastav et al. 2005). Transgenic mice with *Nmt1*-deficient were intercrossed and homozygous *Nmt1*-/- embryos died after 3.5 days, while lower frequency of viable heterozygous *Nmt1*+/- than expected was obtained. Total NMT activity at the early stage of embryonic development was reduced by nearly 95%. *Nmt2* mRNA could be detected at this time but the enzymatic activity was very low, and it has been more important at later stages.

Recent study on *Plasmodium falciparum* (Rahlfs, Koncarevic et al. 2009) demonstrated a putative adenylate kinase, designated as AK2, which has been supposed to be myristoylated by *Pf*NMT. Adenylate kinase is an essential enzyme involving in energy metabolism and macromolecular biosynthesis. By *in silico* search on PlasmoDB, the AK2 gene containing potentially myristoylated sequence was found. The modification of this AK by *Pf*NMT was confirmed by co-expression experiment of the two proteins in *E.coli*, with the presence of myristoyl-CoA. This is the first direct evidence that *Pf*NMT myristoylates an intact malarial protein.

1.3.2 NMT is a therapeutic target

Since many studies have showed that NMT is essential for the development and survival of many human pathogens, it has becomes a potential target for drug development. Most of the achievements have been based on X-ray crystallographic structures of the enzyme in apo-form, or in complexes with substrate, co-substrate and/or inhibitors. Rational drug development based on NMT inhibitor design has not been reported yet. However, homology modeling and/or molecular dynamic simulation studies such as structure-based methods can help in virtual screening or de *novo* designs for discovery of new lead compounds (Sheng, Ji et al. 2009).

In budding yeast, NMT appeared to be highly selective for myristoyl-CoA (MCoA) *in vitro* and *in vivo*. Study of Nmt1p structure with bound MCoA (Wu, Tao et al. 2007) proved that MCoA binds to the enzyme with very high affinity, and the Nmt1p-MCoA complex can be easily co-purified from the expression system. In a study on bovine brain NMT, several synthetic substrates analogs, categorized in two classes: acyl-CoA and non-CoA myristoyl analogs, were tested *in vitro* for inhibition (Glover, Tellez et al. 1991). The first class including *S*-(2-ketopentadecyl)-CoA, *S*-(2-bromo-tetradecanoyl)-CoA and *S*-(3-(epoxymethylene)dodecanoyl)-CoA, and the multi-substrate derivative *N*-(2-*S*-CoA-tetradecanoyl)glycinamide exhibited higher inhibitory activity than the another (1-bromo-2-pentadecanone). All compounds showed reversible competitive inhibition kinetics with respect to myristoyl CoA with K_i values varying from 0.11 to 24 μM.

A variety of compounds were tested for inhibitory activity against NMT in *Leishmania major* and *Trypanosoma. brucei* using indirect discontinuous assay (Panethymitaki, Bowyer et al. 2006). Two compounds, namely CP-030890-27 and CP-014553, showed high inhibitory effect on *Tb*NMT (IC50 values of 250 and 460 nM, respectively) but not on LmNMT (a partial inhibition of 40% was observed at the

same tested concentration as for *Tb*NMT). No other compounds were effective on *Lm*NMT. These inhibitors also had nicely low ED_{50} values, of 66 and 16 μM, respectively against bloodstream *Trypanosoma*, and were non-toxic to murine macrophages in *in vivo* test. These results suggested a promising target, which was NMT, and some anti-trypanocidal candidates for the development of drugs against infectious diseases such as African sleeping disease.

All of the NMTs that have been studied exhibit a preference for myristoyl-CoA than other acyl-CoA derivatives. However, they have divergent peptide substrate specificities. For example, the putative adenylate kinase 2 is supposed to be the unique intact protein target for *Pf*NMT. Therefore, peptide derivatives are more promising and interesting in the attempt to develop species-specific inhibitors for better efficiency against the pathogens.

An imidazole-substituted tripeptide inhibitors against *Candida albicans* NMT was designed and tested (Devadas, Freeman et al. 1997). It exhibited a remarkable selectivity of 560 and 2200-fold toward the fungal NMTs in comparison to the human ones, with an EC50 of 51±17 mM *in vitro*. This kind of peptidic inhibitor appears to bind to the same groove on the enzyme as the non-peptidic benzofuran-cored inhibitor does, as seen in X-ray crystallographic structures. These inhibitors, however, showed different binding mode in terms of the involved amino acids that are critical for binding (Sogabe, Masubuchi et al. 2002).

1.4. Reaction mechanism of NMT

The kinetic studies on NMT have been extensively done on *S. cerevisiae* Nmt1p. Its active form is monomeric without any known co-factor or post-translational modifications. These studies have showed that Nmt1p is highly selective for myristoyl-CoA both *in vitro* and *in vivo*. The common substrates used in these studies are synthetic peptides which are N-terminal derivatives of known N-myristoylated proteins. From these results, some empiric rules have been set to identify known or putative Nmt1p substrates by inferring *S. cerevisiae* genomic data (Farazi, Waksman et al. 2001):

1 - Gly is absolutely required at the +1 position;

2 - Charged residues, aromatics and Pro are not allowed at +2;

3 - All amino acids allowed at +3 and +4

4 - Ser, Thr, Ala, Gly, Cys, or Asn are permitted at +5;

5 - All but Pro are allowed at +6.

Based on these empiric rules, seventy-one Nmt1p substrate ORFs (approximately 1% of the total) were identified. Among these proteins, there was a marked preference for Ser at position +5 (37/71) and for Lys at position +6 (16/71).

The CoA moiety of the acyl substrate is retained in the acyl-NMT complex prior to peptide addition. The catalytic mechanism of NMT is ordered Bi-Bi (Figure 4), in which myristoyl-CoA binding to NMT occurs prior to peptide binding, and CoA

release takes place before the release of acyl peptide [(Bhatnagar, Futterer et al. 1999) and (Rudnick, McWherter et al. 1991)]

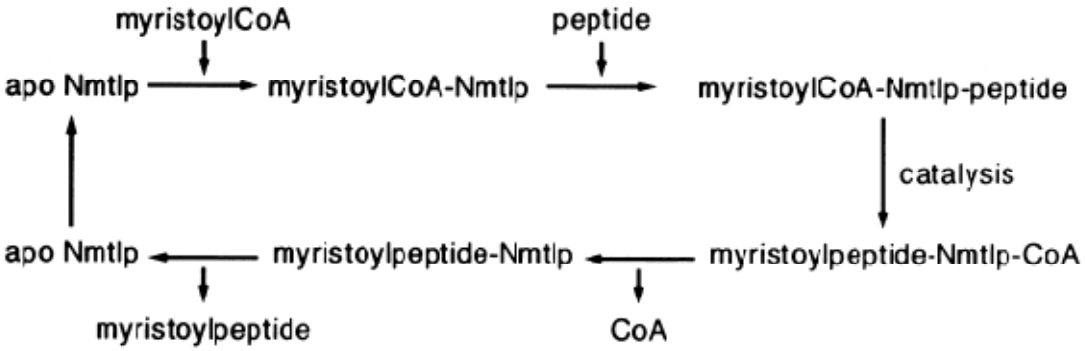

Figure 4: Ordered Bi-Bi reaction mechanism. Binding of MCoA to Nmt1p generates a site for the peptide substrate to bind, and then the chemical transfer of myristate to the N-terminal glycine amine of the peptide occurs. CoA is released followed by the myristoylated peptide

1.4.1 The Nmt1p fold

The Nmt fold consists of a large saddle-shaped β-sheet, which is flanked on both of its faces by several helices. The fold has pseudo two-fold symmetry (Figure 5). The N-terminal half forms the myristoyl-CoA binding site. The only contribution of the C-terminal half to MCoA binding is the side chain of Phe425 (Bhatnagar, Futterer et al. 1999). Although the C-terminal half forms most of the peptide binding site, there are important contacts with residues in αA, βB, and the intervening Ab loop of the N-terminal half (Figure 5) (Bhatnagar, Futterer et al. 1999).

1.4.2 Substrate recognition and binding

According to the crystal structure of binary complex of Nmt1p and bound S-(2-Oxo)pentadecyl-CoA, a myristoyl-CoA analog (Figure 6), the substrate has a question mark-like conformation with four bends at the pyrophosphate group, at C6-C7 of pantetheine, and at C1 and C5-C6 of myristate. As a result, the pantethein and the acyl chain almost encircle the adenine ring. The enzyme itself also forms three features which facilitates the substrate binding (Bhatnagar, Futterer et al. 1999): (1) an oxyanion hole, formed by the main chain amide groups of Phe170 and Leu171, where the thioester carbonyl must be inserted; (2) residues that force a bend at C6 of the acyl chain; and (3) the floor of the acyl chain binding pocket.

An N-terminal 3_{10} helix, namely A', is formed upon MCoA binding. This binding also induces a change in the loop connecting helix A and strand b (Ab loop). The loop then becomes ordered and stabilized, causing the "lid" covering the peptide binding site to be opened (Figure 7). The order of product release is also controlled by the Ab loop [(Bhatnagar, Futterer et al. 1999) and (Farazi, Waksman et al. 2001)].

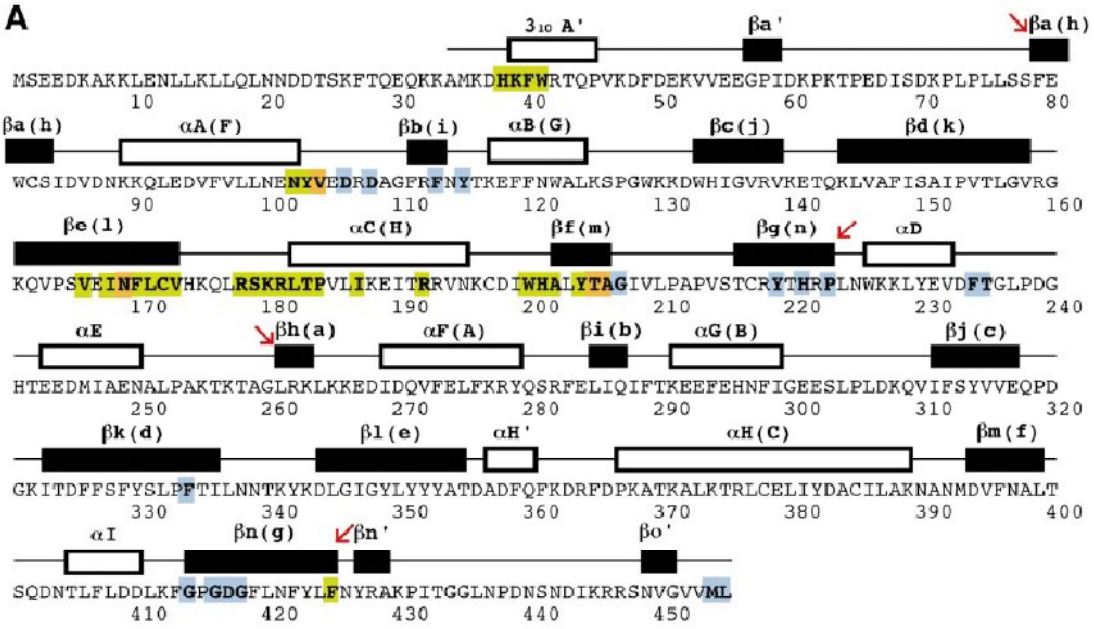

Figure 5: The *S. cerevisiae* Nmt1p fold: Primary sequence of S. cerevisiae Nmt1p with displayed secondary structural elements (α-helices and β-strands). Those designated as primed (e.g., A') are not present in *C. albicans* apo-enzyme. Those indicated in parentheses are symmetric mates of each other (e.g., the symmetric mate of βa(h) is βh(a)). The overall sequence shows a two-fold symmetry in which each half of the protein contains symmetric elements (marked by downward pointing arrows). Residues involved in binding the myristoyl-CoA analog, dipeptide inhibitor and in interaction with both (according to the results of inhibitory experiments done by (Bhatnagar, Futterer et al. 1999) are shown in lime, blue and orange, respectively.

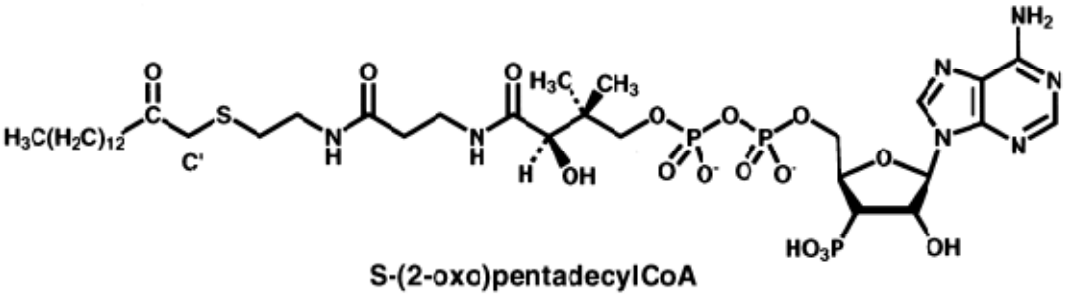

Figure 6: Structure of S-(2-Oxo)pentadecyl-CoA, a myristoyl-CoA analog and a competitive inhibitor of Nmt1p (K_i = 5 nM). This nonhydrolyzable acyl-CoA since it has an additional methylene (C') between the sulfur of CoA and the carbonyl carbon of the myristate moiety.

1.4.3 Catalytic mechanism

The myristoyl moiety from MCoA is transferred to the N-terminal glycine of the peptide substrate via a nucleophilic addition-elimination mechanism (Figure 8) (Bhatnagar, Futterer et al. 1999). The main chain amides of Phe170 and Leu171 form an oxyanion hole where the thioester carbonyl of MCoA is positioned and polarized with a partial positive charge on the carbon. Binding of myristoyl-CoA orders and

stabilizes the flexible Ab loop, and generates a fully functional peptide binding site. The N-terminal glycine nitrogen of the nascent peptide, which is predominantly in protonated form ($NH_3^{+)}$, is a poor nucleophile at physiological pH. This ammonium group faces the C-terminal carboxylate group of Leu455 and gets deprotonated upon peptide binding. The resulting amine now becomes a potential nucleophile to attack the thioester carbonyl.

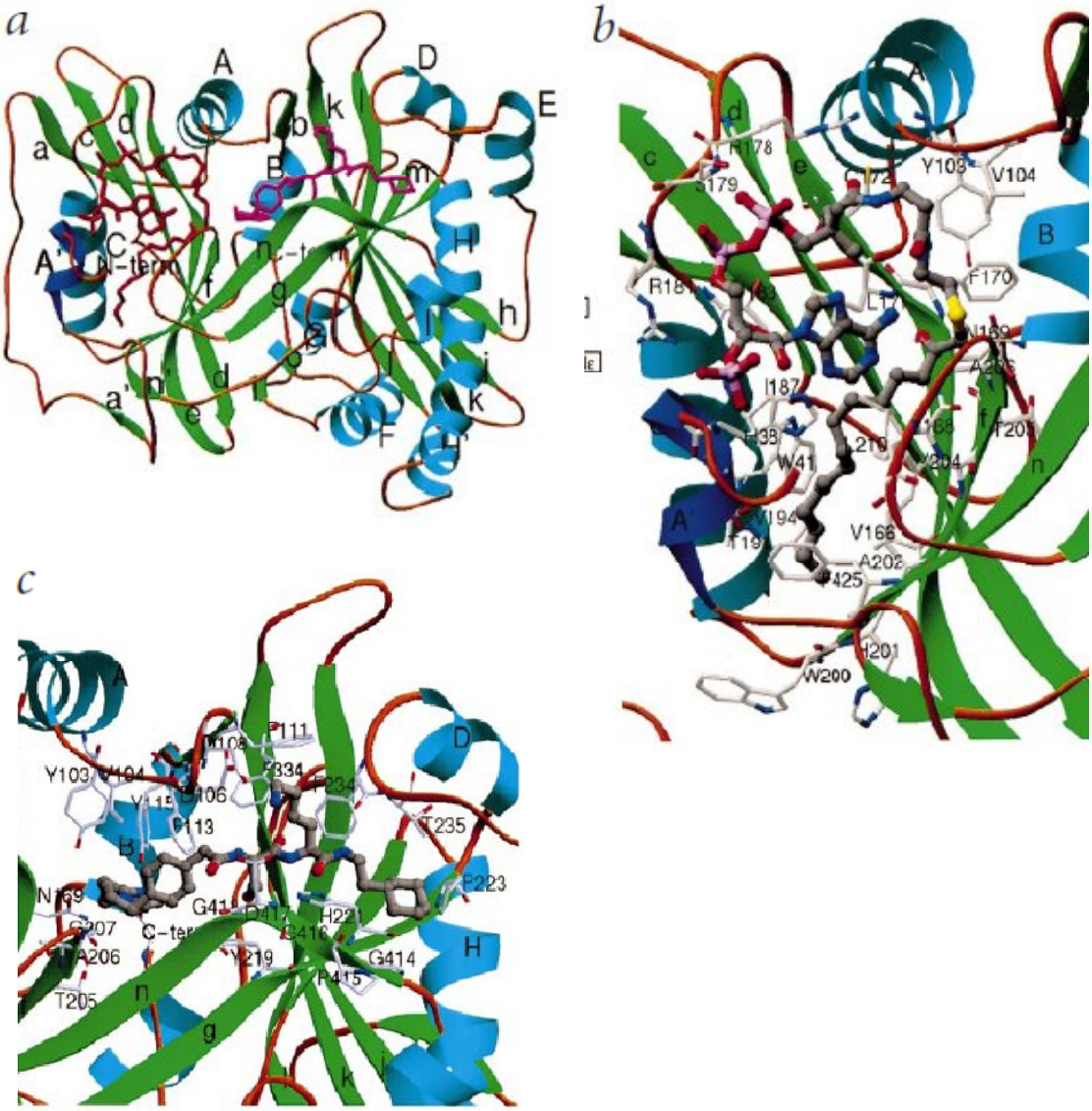

Figure 7: Contacts between Nmt1p and its substrates. (a) Nmt1p structure with bound S-(2-oxo)pentadecylCoA (red) and peptide substrate (magenta). (b) Binding site of S-(2-oxo)pentadecylCoA and Nmt1p. The MCoA analog adopts a question mark-like conformation upon binding. The main chain of Phe170 and L171 of the enzyme forms an oxyanion hole in which the thioester carbonyl of MCoA analog is inserted. (c) Binding site of peptide (GLYASKLS) and Nmt1p. Secondary structure elements color coding: α-helices, 3_{10}-helices, strands and loops are light blue, deep blue, green and amber respectively. Atoms color coding: carbon, grey; oxygen, red; phosphorus, purple; nitrogen, blue; and sulfur, yellow. The substrates is drawn in larger bonds (a darker shade of grey is used for its carbon atoms)

Acyl transfer proceeds through formation of a tetrahedral reaction intermediate, which is stabilized by the oxyanion hole together with the H-bonding network (Farazi, Waksman et al. 2001). Subsequent collapse of the tetrahedral intermediate leads to extrusion of CoA. From the X-ray crystallographic data, the Gly1 amine seems to be rotated 180° around the ψ. During this process, the Gly1 amine is deprotonated, whereas the thiolate group of CoA is re-protonated, presumably through proton exchange between these two groups. The thiolate group is stabilized by the N-6 amine of the CoA adenine. This intra-molecular stabilization mechanism accounts for the bent conformation of CoA (Farazi, Waksman et al. 2001). The C-terminal carboxylate of Nmt1p is then deprotonated (presumably by solvent contact) to start the next catalysis turn.

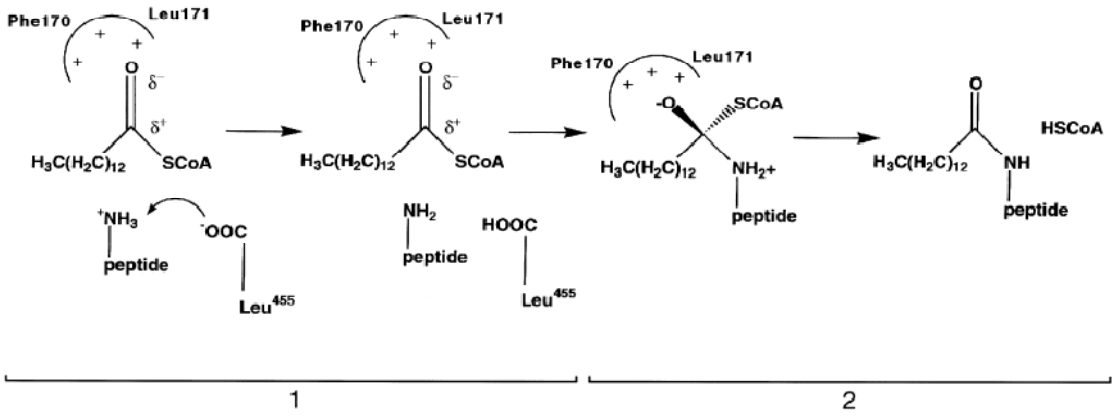

Figure 8: Summary of Nmt1p catalytic mechanism.

(1) The thioester carbonyl of MCoA is firstly polarized inside the oxyanion hole to make the carbon attractive for nucleophilic attack. The N-glycine ammonium is also deprotonated by the carboxylate of C-terminal Leu455 to form a nucleophilic amine. Hydrogen bonding interactions between the Gly-1 amine with Asn-169 and Thr-205 residues of Nmt1p position the amine along the reaction trajectory and facilitate nucleophilic attack.

(2) The oxyanion hole together with the H-bonding network stabilizes the developing tetrahedral intermediate. Following acyl transfer, free CoA is released. This event disorders the Ab loop and 3_{10} A' helix, leading to the release of the myristoyl peptide product.

Steady state kinetics studies combined with the X-ray crystallographic studies of the binary and ternary Nmt1p complexes suggest that the rate-limiting step in the reaction is an isomerization step. The isomerization could involve reversal of the changes that occur upon myristoyl-CoA binding, *i.e.* disordering of the N-terminal 3_{10} A' helix and altering the conformation of the Ab loop (Farazi, Waksman et al. 2001).

Those results reveal that the chemical transfer occurs by main chain atoms: the oxyanion hole formed by the main chain amide groups of Phe170 and Leu171, and the carboxylate of Leu455. Moreover, Nmt1p is also the first reported enzyme that has the C-terminal carboxylate group involved in catalysis (Bhatnagar, Futterer et al. 1999).

1.5. *Plasmodium falciparum* N-myristoyltransferase (*Pf*NMT)

There are many crystallographic structures of NMT from five species that have been reported: *Saccharomyces cerevisiae* [(Bhatnagar, Futterer et al. 1998) and (Wu, Tao et al. 2007)], *Candida albicans* [(Sogabe, Masubuchi et al. 2002) and (Weston, Camble et al. 1998)], *Trypanosoma brucei* (Frearson, Brand et al. 2010), and *Leishmania donovani* (Brannigan, Smith et al. 2010). However, no structure of *Pf*NMT has been available yet.

NMT is a single-copy gene in *P. Falciparum,* and it is expressed in the asexual blood stages of the malarial parasite's life cycle. The full-length *Pf*NMT cDNA ORF contains 1230 bp, with the potential to encode a 48 kDa protein. An alignment of orthologous NMT sequences showed that the *P. falciparum* enzyme has extensive sequence conservation in the central and C-terminal regions of the protein, whereas there is most diversity at the N-terminus. Most of the residues, which are known to participate directly in the enzymatic mechanism or play critical regulatory roles in yeast NMT, are conserved in the *Pf*NMT (Gunaratne, Sajid et al. 2000)

ADP-ribosylation factor 1 (ARF1) was identified to be a potential substrate for *Pf*NMT (Stafford, Stockley et al. 1996). Another putative substrate has recently been identified and designated as adenylate kinase 2 (AK2) (Rahlfs, Koncarevic et al. 2009).

Recombinant *Pf*NMT could be expressed in *E.coli* in enzymatically active form (Gunaratne, Sajid et al. 2000). The recombinant protein had an N-terminal 6xHis-tag and could be purified using a nickel-chelate column. Although the protein expression level was not very high (12 μg per liter of culture) due to condon usage bias, it showed a considerable activity on synthetic peptide (N-terminal derivative of ARF1). *Pf*NMT expressed in *E. coli* was not inhibited by 10 mM iodoacetamide or 10 mM DEPC, while human NMT activity was inhibited by 50% and 5%, respectively (Gunaratne, Sajid et al. 2000).

Part 2: Aims of Research Project

The project dealt with the expression and purification *Pf*NMT. The purified *Pf*NMT was used for crystallization to exploit its structure. The kinetics of N-myristoylation was also studied *in vitro*.

In detail, the practical work consisted of:

- Optimization for *Pf*NMT over-expression, with an N-terminal 6x His-tag, in *E. coli*.
- Establishment an optimal strategy for *Pf*NMT purification using several chromatographic techniques.
- Crystallization trial set up for three-dimensional structure solving by X-ray crystallography.
- *In vitro* kinetic study of *Pf*NMT (with and without His-tag) on synthetic myristoyl-CoA and peptide substrate using biochemical enzymatic assay and Isothermal Titration Calorimetry (ITC).

Part 3: Results

3.1. Expression of recombinant *Pf*NMT

*Pf*NMT ORF was cloned in pET28 vector, namely pET28-His-*Pf*NMT, with the N-terminal 6xHis tag (Figure 9), and was confirmed by DNA sequencing. The encoded *Pf*NMT had predicted molecular weight and theoretical pI of 51,514 Da and 8.64, respectively. Those of NMT without the His tag were 47,970 Da and 8.39, respectively. These predicted characteristics were calculated using the Online ExPASy Proteomics tool (http://www.expasy.ch/tools/pi_tool.html)

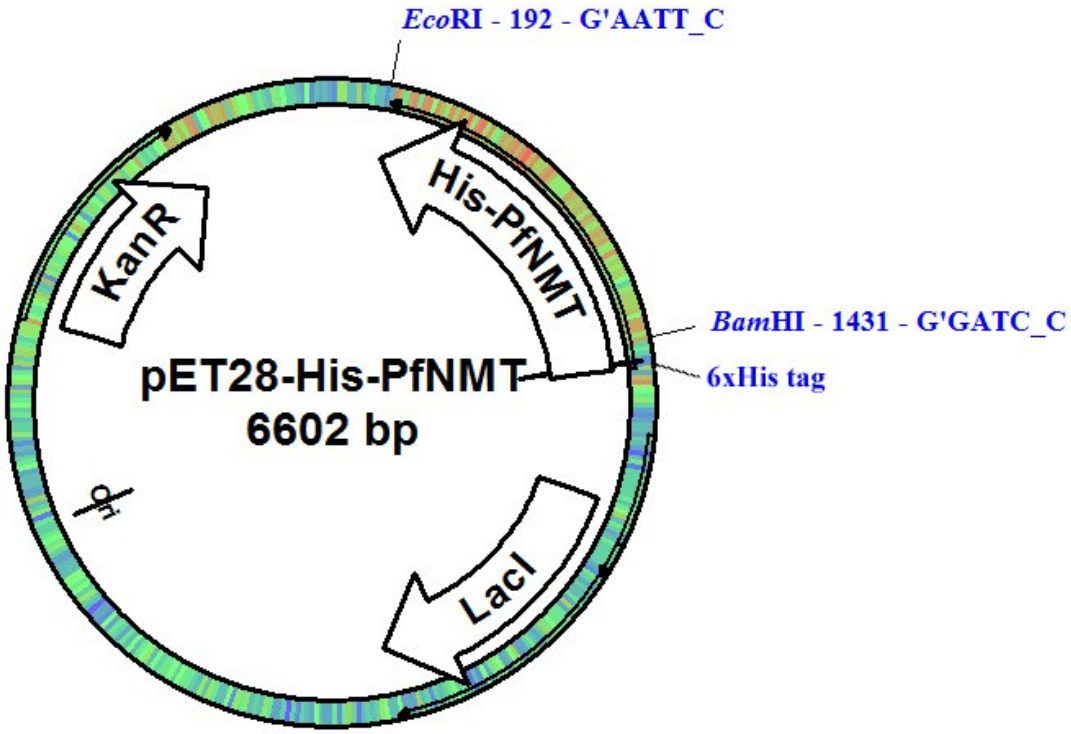

Figure 9. *Pf*NMT cloned into pET28 vector containing a N-terminal 6x-His tag, designated as His-*Pf*NMT. The construct has a kanamycine-resistant (KanR) gene as a selective marker

At the beginning, a standardization experiment of the culture condition was done to achieve optimal expression. The *E. coli* cells were grown at 37^0C in three different media: LB, 2xYT and TB in a volume of 20 mL for each condition. As soon as the OD_{600} reached 0.5-0.6, the cultures of each medium were induced with 3 different concentrations of IPTG: 0.1 mM, 0.3 mM or 1 mM IPTG. Finally, they were continually grown at two temperatures: 28^0C and 37^0C for 6 hours. The yield of His-*Pf*NMT was relatively derived from western blot analysis (Figure 10).

His-*Pf*NMT expression at 37^0C resulted in less protein with more impurities (Figure 10), which was not efficient for further purification. The major impurities have

molecular weights of 20 and 25 kDa. There was almost no difference in the expression when induced with 0.3 mM or 1 mM IPTG. In short, His-*Pf*NMT could be expressed at highest level in 2xYT medium induced with 0.3 mM IPTG at 28^0C (Figure 10). These conditions were used for large scale production of the recombinant His-*Pf*NMT.

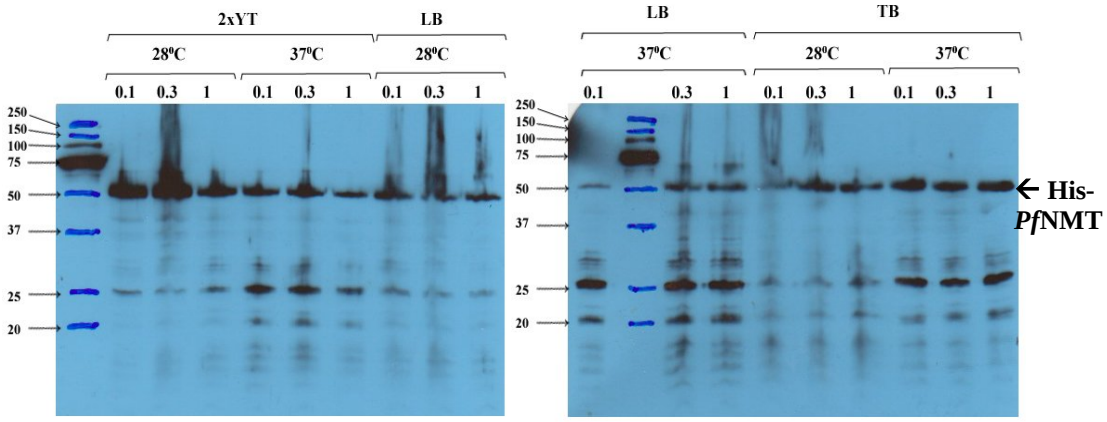

Figure 10. Western blot analysis of total cell proteins (TCP) in different culture condtions. Three media (2xYT, LB and TB), three concentration of IPTG for induction (0.1, 0.3 and 1 mM) and two temperatures (28^0C and 37^0C) for post-induction culture were examined. His-*Pf*NMT was detected by anti-6xHis antibody. The band at about 51 kDa corresponded to His-*Pf*NMT. More impurities were seen in TCP at 37^0C in all other conditions.

In large-scale culture, e.g. five or ten liters, TCP before and after IPTG induction was examined to be sure there would be no leaky expression. Western blotting result (Figure 11) clarified that the expression was good as the band of His-*Pf*NMT had been detected in only post-induced TCP.

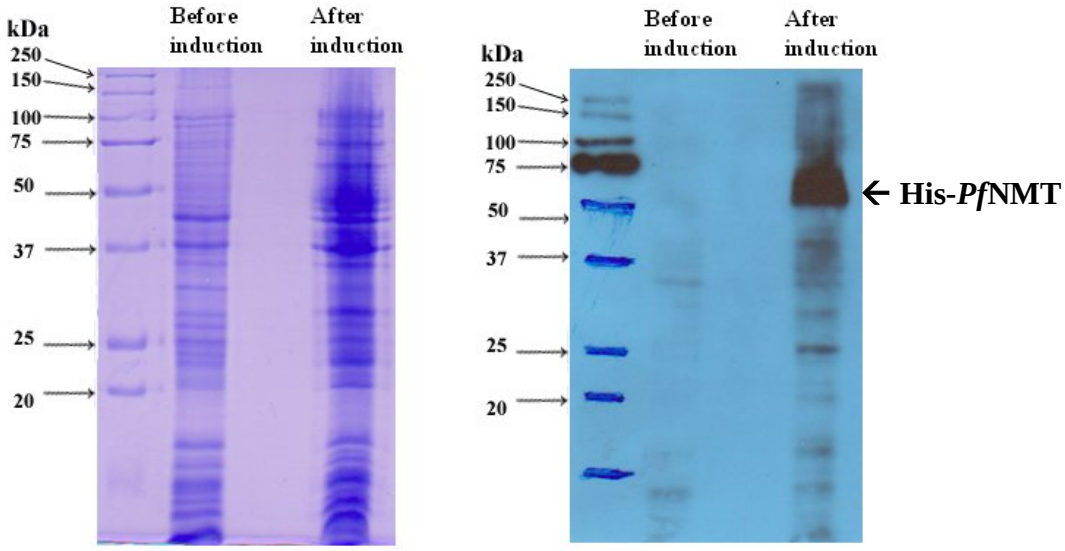

Figure 11. Expression analysis of large-scaled His-*Pf*NMT production. TCPs from 10 liters of culture before and after induction were run on SDS-PAGE (*Left panel*) and then Western-blotted (*Right panel*). His-*Pf*NMT was nicely expressed at the chosen condition

3.2. Purification of His-*Pf*NMT

3.2.1 First strategy: IMAC – SEC - IEX

The recombinant *Pf*NMT was partly purified by affinity chromatography on the Nickel-Sepharose column, subsequently by size exclusion and cation exchange chromatography. On Nickel-sepharose column, a washing step with 5% imidazole (12.5 mM) was done after loading, and then a continuous gradient of imidazole concentration (0-250 mM) was applied to elute the 6xHis-tagged NMT. One single peak was obtained and fractionated in 1 mL sized-fractions (Figure 12). The purity of these fractions were shown in Figure, the band of His-*Pf*NMT was about 51 kDa.

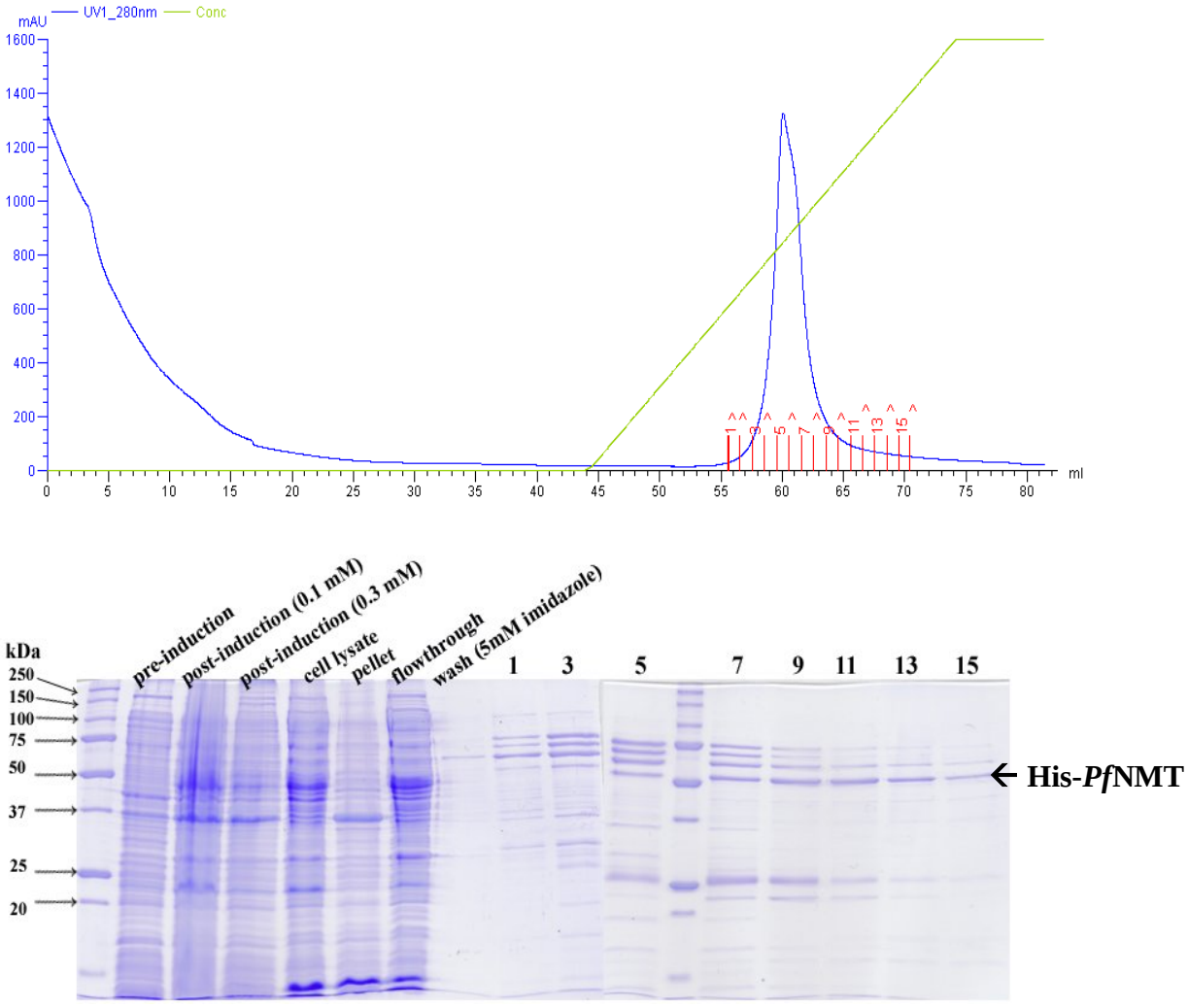

Figure 12. Immobilized metal affinity chromatography (IMAC) on Nickel-Sepharose column to purify His-*Pf*NMT. The purification comprised sample loading, washing at 5 mM imidazole and eution step. *Upper panel*: Chromatogram with the recorded absorbance at 280 mm (blue curve) and the continuous gradient of imidazole (5-250 mM) (green curve) to elute binding protein. Fraction size was 1 mL each. *Lower panel*: SDS-PAGE analysis of IMAC purification including: TCP before and after IPTG induction, cell lysate and pellet after sonication, and fractions (1-15) after loading on Nickel-Sepharose column.

Washing with 5 mM imidazole was insufficient to deplete all unspecifically bound proteins, as seen in Figure 12. Therefore, a step-wise gradient was applied instead. In a small-scaled preparative experiment, the gradient comprised 5%, 15%, 25%, 35%, 45% and 100 % elution buffer. Washing with 15% elution buffer (or 37.5 mM imidazole) could help remove most impurities; and His-*Pf*NMT started to be eluted at 25% of elution buffer, equivalently to 62.5 mM imidazole (Figure 13). Therefore, 40 mM imidazole had been included in the IMAC binding buffer from then on for later His-*Pf*NMT purifications on Nickel-sepharose column.

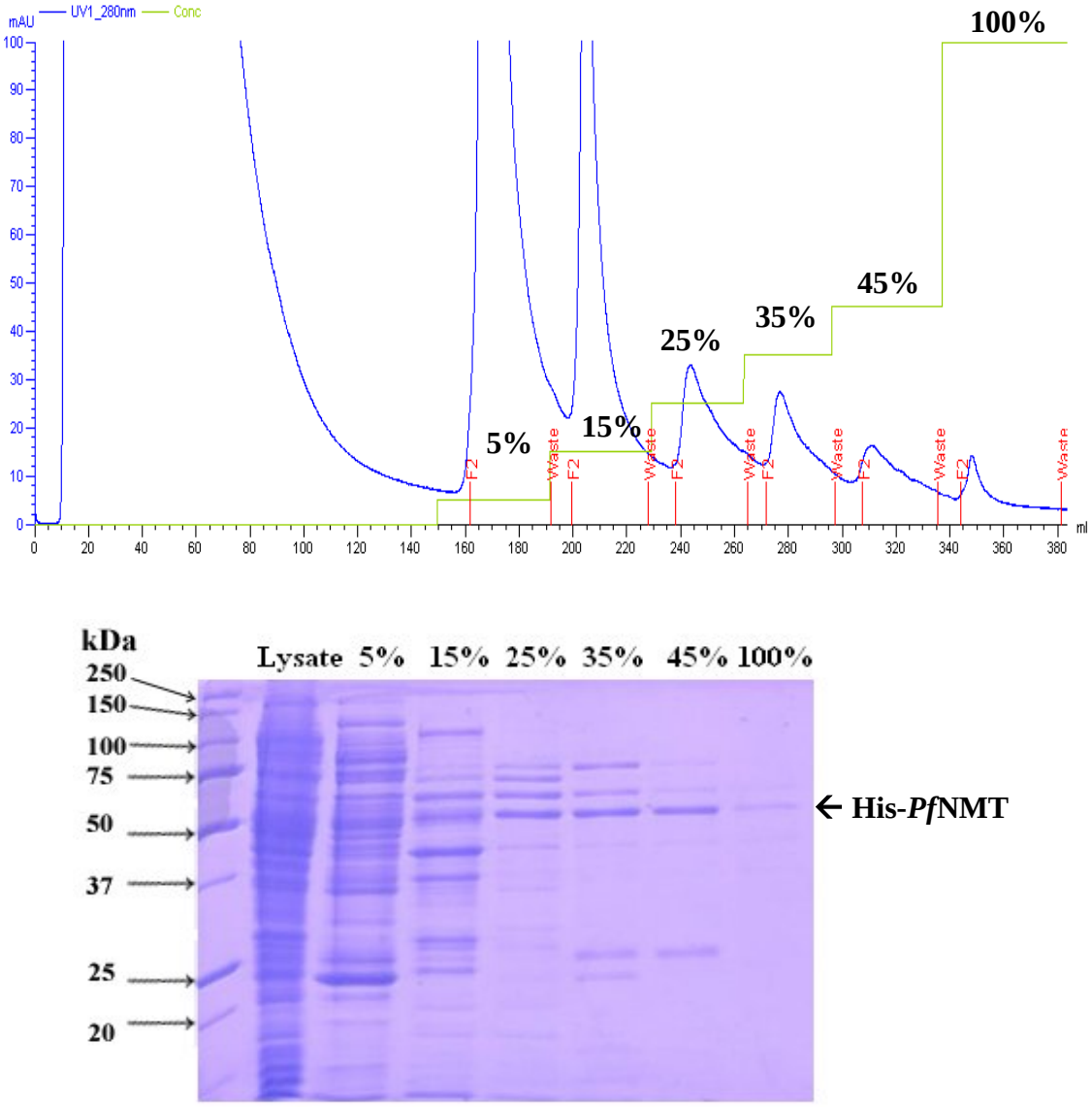

Figure 13. Immobilized metal affinity chromatography (IMAC) on Nickel-Sepharose column to purify His-*Pf*NMT. The purification comprised sample loading, washing at 5 mM imidazole and eution step. *Upper panel*: Chromatogram with the recorded absorbance at 280 mm (blue curve) and the continuous gradient of imidazole (5-250 mM) (green curve) to elute binding protein. *Lower panel*: SDS-PAGE analysis of IMAC purification including: TCP before and after IPTG induction, cell lysate and pellet after sonication, and fractions after loading on Nickel-Sepharose column.

All fractions containing His-*Pf*NMT were pooled and concentrated to 1 mL for loading on size exclusion column. Firstly, the Superdex 75 column was used. It exhibited a poor resolution since the peak of void volume much overlapped with the peak of His-*Pf*NMT. Moreover, this protein appeared to be likely multiple bands after passing through the column (Figure 14A), which was not observed when using the Superdex 200 column. The Superdex 200 also gave better resolution (Figure 14B). His-*Pf*NMT peak had the retention time of about 80 min on Superdex 200 column. The fractions with His-*Pf*NMT were pooled together and loaded on cation exchange column (Mono S) in the next step.

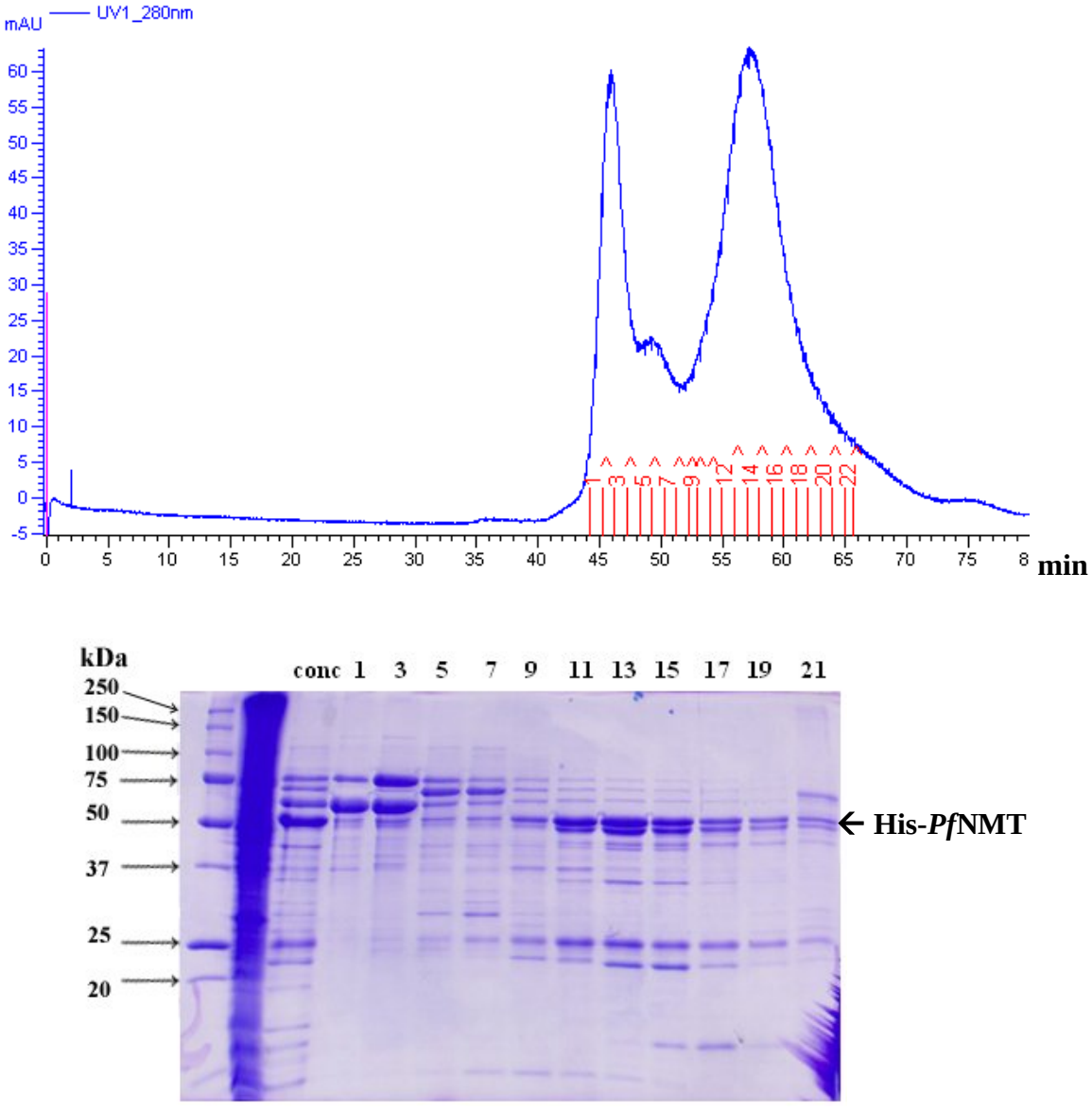

Figure 14A. Size exclusion chromatography of the concentrated Nickel-Sepharose eluent (conc) on Superdex 75 column. The chromatogram showed quite poor resolution of the proteins (*Upper panel*). Eluted proteins were collected in 1 ml-sized fractions.SDS-PAGE analysis of eluted fractions (1-21) indicated multiple bands of His-*Pf*NMT after passing through the column (*Lower panel*).

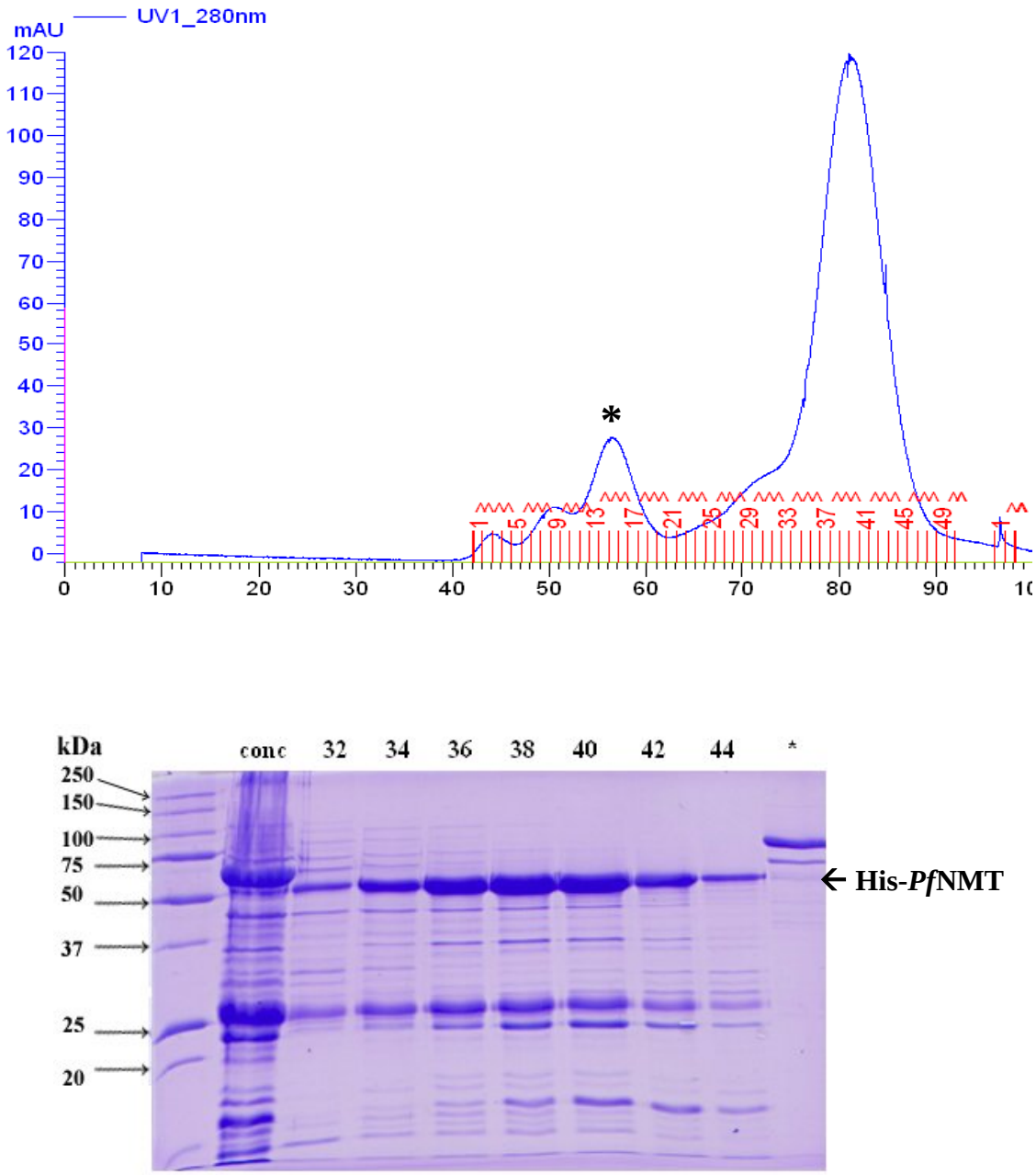

Figure 14B. Size exclusion chromatography of the concentrated Nickel-Sepharose eluent (conc) on Superdex 200 column. It gave a better resolution than using Superdex 75 column (*Upper panel)*. Moreover, no multiple bands of His-*Pf*NMT were observed after running (*Lower panel*), (*) was pooled from all fractions that have retention time less than 65 min

There was almost no protein coming out in the flowthrough when loading on Mono S column (Figure 17). His-*Pf*NMT was eluted using a continuous gradient from 0.1 M to 1 M NaCl. At least three peaks of proteins were obtained, and both of them seemed to contain NMT. Only the fractions of the major peak were collected. The protein amount, determined by Bradford assay, was approximately 285 mg per 5 liters of culture, which was still too low.

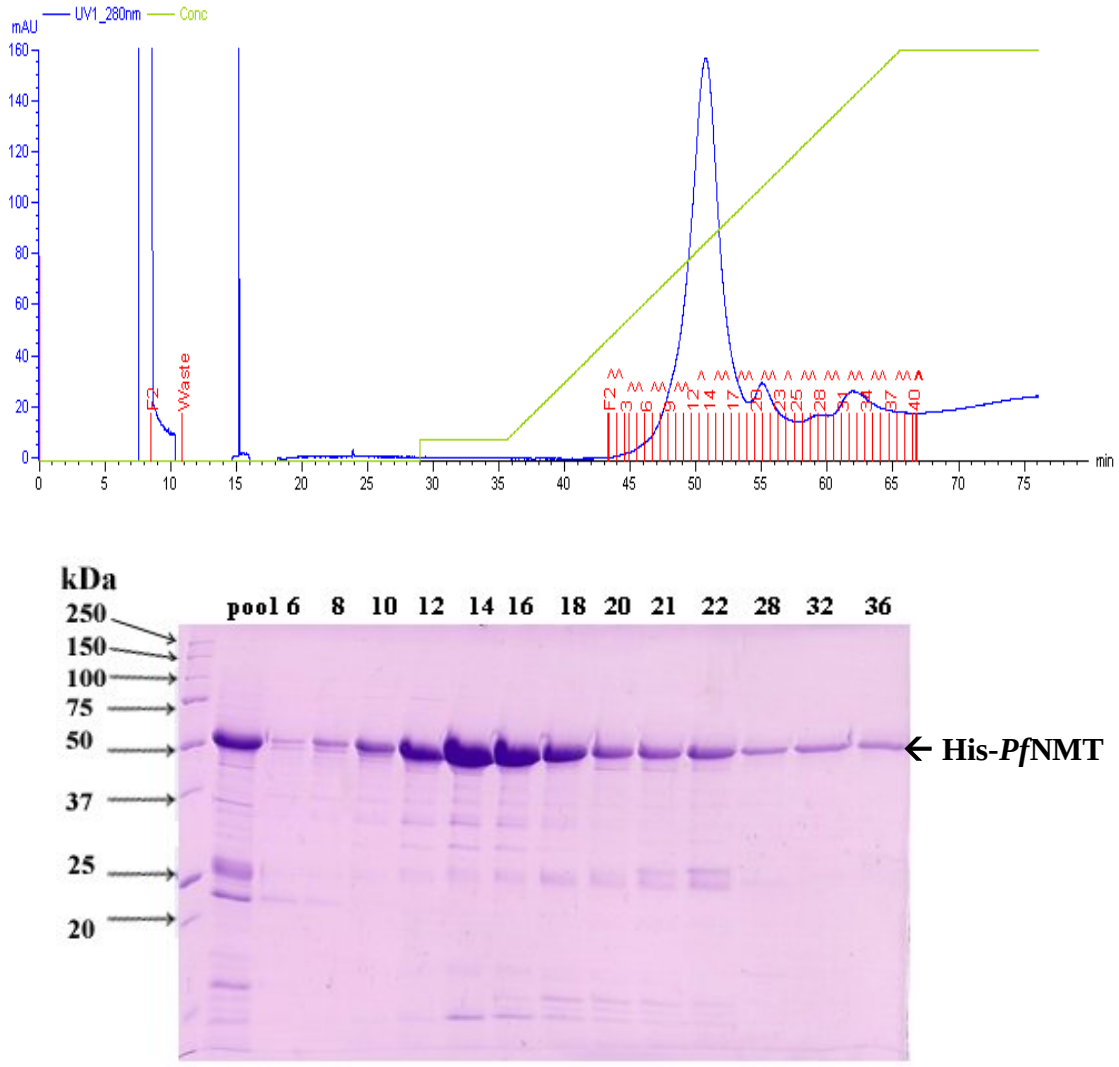

Figure 15. Cation exchange chromatography on Mono S column. *Upper panel*: chromatogram with loading path, washing step with 5% elution buffer (0.145 M NaCl), and continuous eluting concentration gradient of NaCl (0.1 – 1 M). Fraction size was set at 0.33 mL each. *Lower panel*: SDS analysis of eluted fractions. 'pool' means the samples pooled from SEC step on Superdex 200 column. Other factions were taken alternatively from 8 to 36

3.1.2 Second strategy: IMAC – Desalting – IEX – SEC

In order to achieve more efficient purification, another strategy was conducted, starting with affinity chromatography on Nickel-Sepharose column as usual. This time, the binding buffer was supplemented with 40 mM imidazole; and hence unspecifically bound proteins would be washed out during loading time. Then the imidazole concentration was raised to 250 mM to elute the bound proteins (Figure 16A). Subsequently, a desalting step was applied to exchange the buffer so that the protein mixture was in the IEX binding buffer and was ready for cation exchange purification. There was no different from the eluting profile when using the first strategy. The desalting step resulted in two times increasing of the sample volume. On the SDS-PAGE gel, the NMT band intensity was almost half of that before desalting.

This means that there was no protein loss since equal volume of the samples was loaded on the gel (Figure 16B).

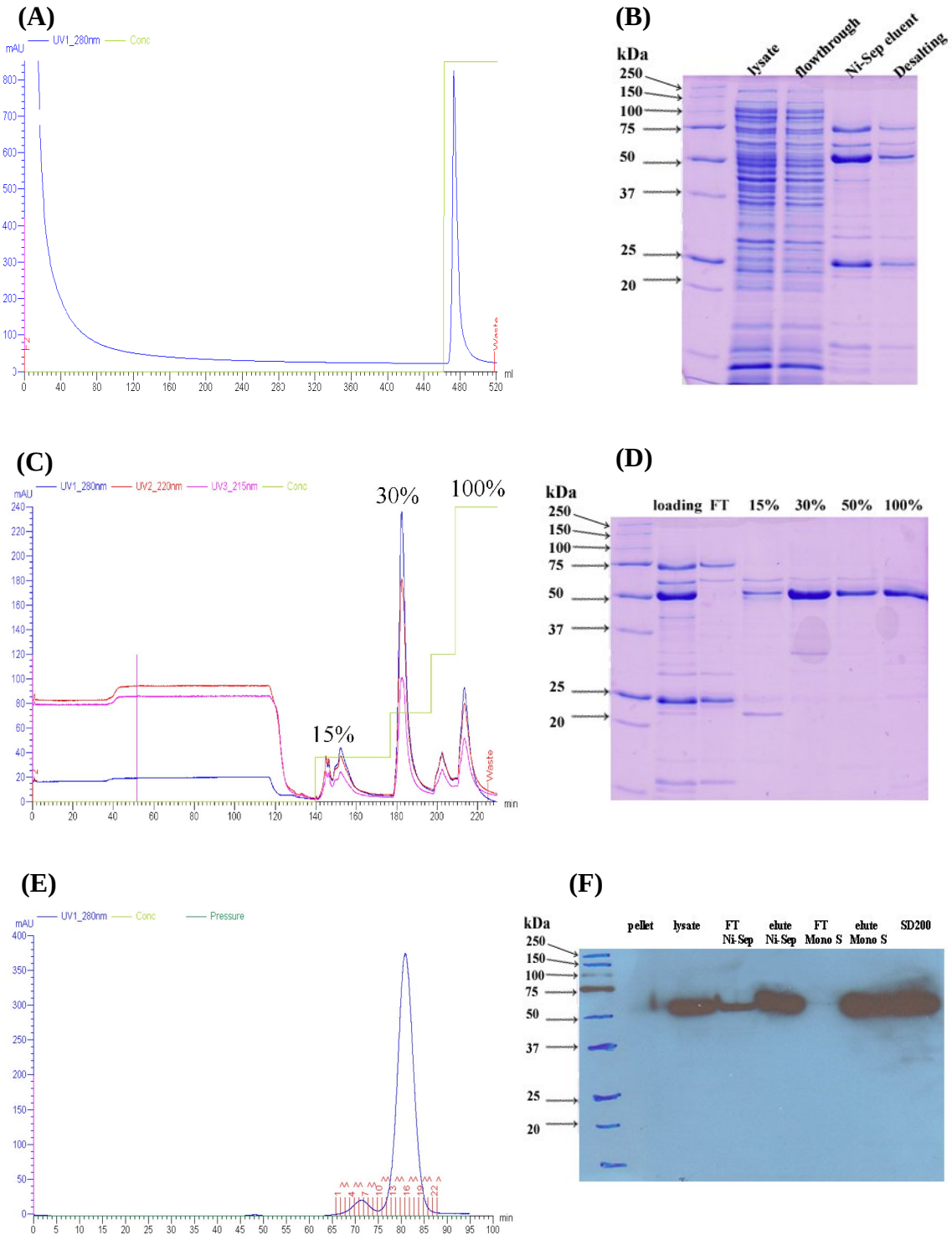

Figure 16. Another strategy for His-*Pf*NMT purification comprising 4 steps: IMAC – Desalting – IEX – SEC. (A) IMAC on Nickel-Sepharose column. There was no longer the washing step since the 40 mM imidazole was already included in binding buffer. (B) SDS-PAGE of IMAC purification and desalting. (C) IEX on Mono S column with a step-wise gradient elution. The major peak containing His-*Pf*NMT was eluted at 30% elution buffer (or 0.55 M NaCl). (D) The SDS-PAGE result indicated that recombinant NMT was also present in the two later eluents at

50% and 100% elution buffer. (E) Chromatogram of SEC after IEX represented a major peak containing His-*Pf*NMT. (F) Western blotting analysis of the whole purification process. There was no NMT in the cell pellet but a partial loss during IMAC in which NMT came in the flowthrough.

Similarly, the appliance of a step-wise gradient on Mono S column yielded better separation of His-*Pf*NMT from other proteins (Figure 16C). Non-specific binding proteins were washed with 15% of elution buffer (or 0.235 M NaCl), and the His-*Pf*NMT-containing peak was eluted at 30% of elution buffer (or 0.37 M NaCl) (Figure 16C). The whole eluent was collected and concentrated. There were two additional peaks, eluted at 0.55 M and 1 M NaCl, respectively, in which His-*Pf*NMT was present as well (Figure 16C and 16D).

The IEX eluent was concentrated and loaded on Superdex 200 column to remove any aggregation form of proteins. A small peak of impurities came out before the peak of His-*Pf*NMT (Figure 16E). All fractions with NMT were pooled together and concentrated to approximately 18 $mg.ml^{-1}$ for crystallization trial. The overall purification process was evaluated by Western blot (Figure 16F). Although the purity looked better than that from the first purification strategy; there was, however, a major impure band of about 25 kDa present (Figure 16G).

Treatment of *Pf*NMT with thrombin to cleave the His tag was done. The His-*Pf*NMT was incubated with thrombin (amount according to the manufacturer) overtime. The digestion profile (Figure 16H) showed that the cleavage was almost completed after 12 hours at room temperature.

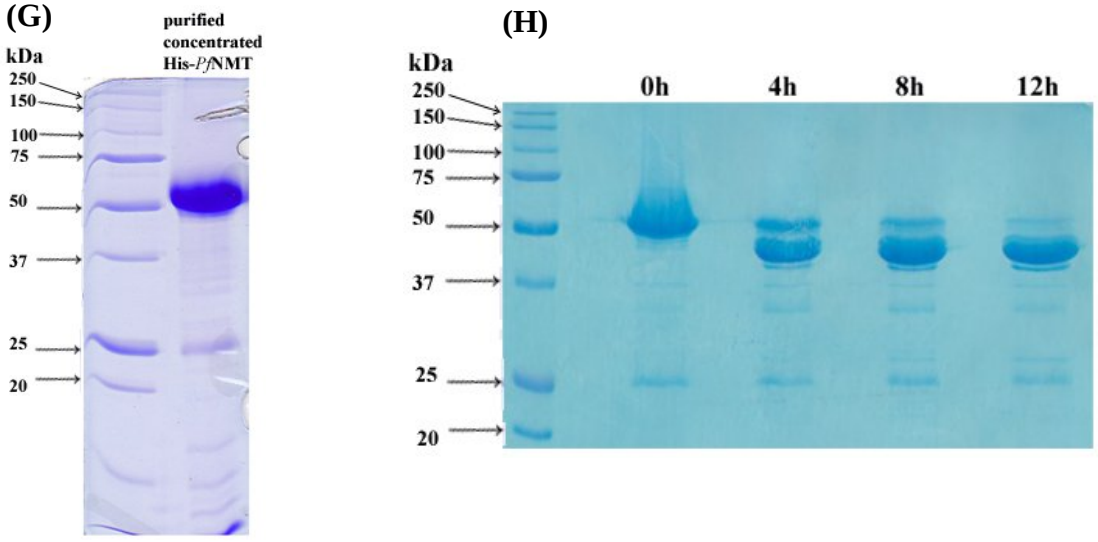

Figure 16 (continued). (G) The purified His-*Pf*NMT collected and pooled from the SEC on Superdex 200 column was concentrated to 18 $mg.ml^{-1}$. The major impurity was a protein with molecular weight of about 25 kDa. (H) Thrombin digestion profile of purified His-*Pf*NMT. The protein was incubated with thrombin at room temperature. One microliter of the mixture was taken out after 0, 4, 8 and 12 hours and analyzed in SDS-PAGE gel

3.3. Enzymatic assay

3.3.1 Michelis-Menten modeling

The data collected from enzymatic assay on a range of synthetic octapeptide concentration were fitted into Michaelis-Menten kinetics model by using GraphPad Prism software. The K_m values of *Pf*NMT before and after removal of the tag were determined as 551 and 693 μM, respectively. The specific activity of both types of *Pf*NMT, illustrated by the V_{max} values, was more or less similar (Figure 17). The activity of NMT was not detected in the absence of the enzyme itself, myristoyl-CoA or the peptide substrate (BSA was used as control).

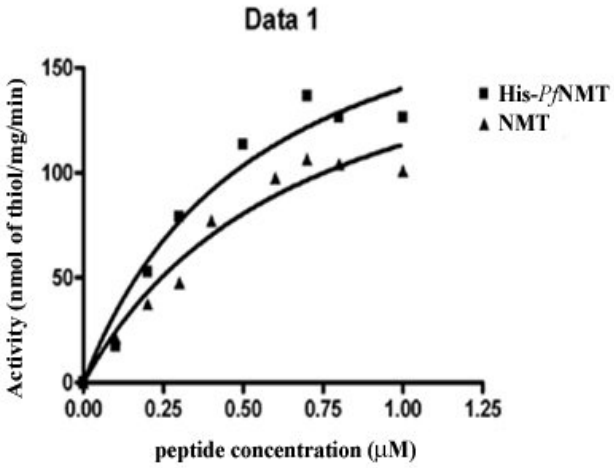

(A)

	His-NMT	NMT
Best-fit values		
Vmax	217.5	192
Km (mM)	0.5514	0.6926
Std. Error		
Vmax	38.97	36.58
Km	0.2088	0.2511
95% Confidence Intervals		
Vmax	122.2 to 312.9	105.5 to 278.5
Km	0.04049 to 1.062	0.09876 to 1.287
Goodnes of Fit		
Degree of fredom	6	7
R^2	0.9591	0.9600
Absolute Sum of Squares	804.1	518.1
Sy.x	11.58	8.603
Data		
Number of X Values	10	10
Number of Y replicates	1	1
Total number of values	8	9
Number of missing values	2	1

(B)

Figure 17. Kinetic analysis of *Pf*NMT. Both tagged and non-tagged *Pf*NMT were examined. (A) Michaelis-Menten curves generated by fitting the enzymatic assays data on a range of peptide concentration into non-linear regression. (B)Statistic analysis of the achieved data set, also done by GraphPad Prism software

3.3.2 pH and temperature optimum

The effects of pH and temperature to the enzyme activity were examined. In a narrow pH range from 6.0 to 8.5, *Pf*NMT exhibited a preference of slight acidity for its activity. The optimal pH was determined as 6.5 (Figure 18A). *Pf*NMT almost lost 50% of its activity at pH 8.5.

The temperature dependency of the enzyme activity was also investigated. It appeared to be less active at temperature lower than 30^0C, and reach the maximum activity at 37^0C. Above this temperature, the enzyme was quickly inactive (Figure 18B).

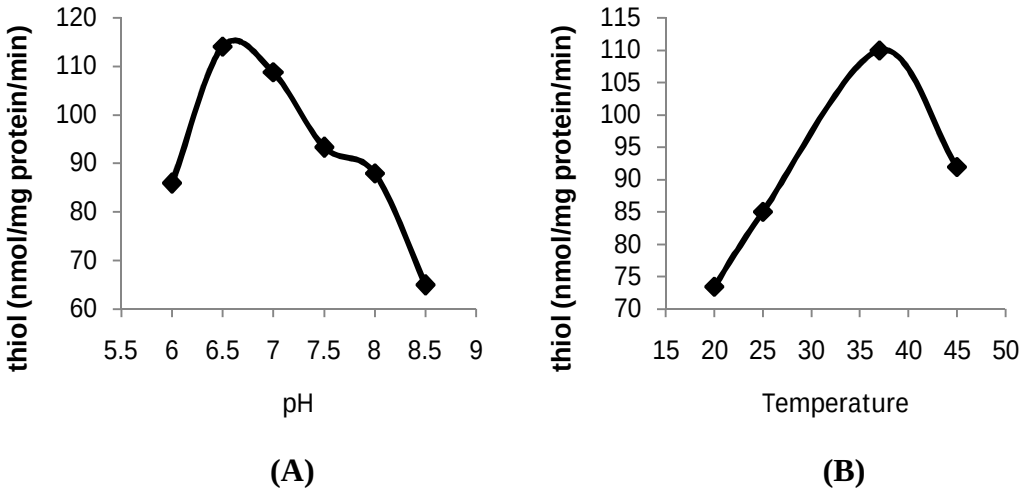

Figure 18. pH and temperature dependency study of His-*Pf*NMT (A). The enzyme exhibited highest activity at pH 6.5 and 37^{0}C (B)

3.3.3 Isothermal titration calorimetry

The interaction of the peptide substrate to *Pf*NMT was investigated. There was no binding of the peptide to the enzyme without the presence of myristoyl-CoA since only the background level of the titration curve was observed (Figure 19A). It was, however, weird that myristoyl-CoA also did not exhibit any interaction with *Pf*NMT (Figure 19B), which had been supposed to occur prior to the binding of the peptide substrate.

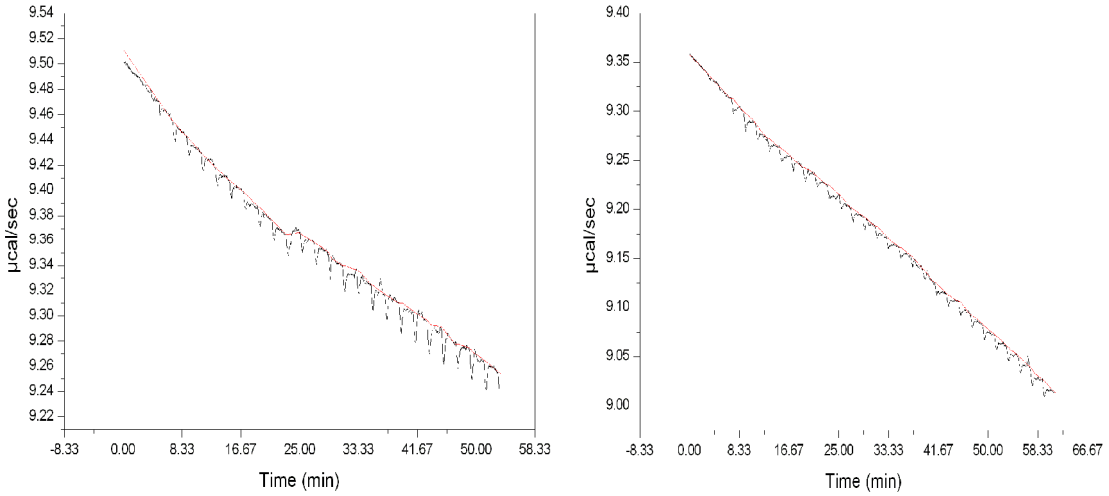

Figure 19. Isothermal titration calorimetry experiment to investigate the interaction between His-*Pf*NMT and its substrate. (A) Titration of myristoyl-CoA and (B) of the synthetic octapeptide to apo-His-*Pf*NMT. Both showed no binding

3.4. Crystallization trial

The crystallization screening was carried out using Hampton HR2 110 and HR2 112 Crystal Screen Kits as initial starting. After 4 weeks, the observation was recorded as in Table 1. There was no hit achieved through this screening.

Table 1: Crystallization screening using Hampton HR2 110 and HR2 112 Crystal Screen Kits. Interpretation: P: precipitate, C: clear, PH: phase separation

	Crystal Screen™ - HR2-110 Sample concentration: 15 mg.ml Drop formula: (0.5 µl samle + 0.5 µl reservoir) against 500 µl resevoir	Interpretation		
1	0.02 M Calcium chloride dihydrate, 0.1 M Sodium acetate trihydrate pH 4.6, 30% v/v (+/-)-2-Methyl-2,4-pentanediol	P		
2	0.4 M Potassium sodium tartrate tetrahydrate	P		
3	0.4 M Ammonium phosphate monobasic	P		
4	0.1 M TRIS hydrochloride pH 8.5, 2.0 M Ammonium sulfate		C	
6	0.2 M Magnesium chloride hexahydrate, 0.1 M TRIS hydrochloride pH 8.5, 30% w/v Polyethylene glycol 4,000	P		
7	0.1 M Sodium cacodylate trihydrate pH 6.5, 1.4 M Sodium acetate trihydrate		C	
8	0.2 M Sodium citrate tribasic dihydrate, 0.1 M Sodium cacodylate trihydrate pH 6.5, 30% v/v 2-Propanol		C	
9	0.2 M Ammonium acetate, 0.1 M Sodium citrate tribasic dihydrate pH 5.6, 30% w/v Polyethylene glycol 4,000	P		
10	0.2 M Ammonium acetate, 0.1 M Sodium acetate trihydrate pH 4.6, 30% w/v Polyethylene glycol 4,000	P		
11	0.1 M Sodium citrate tribasic dihydrate pH 5.6, 1.0 M Ammonium phosphate monobasic	P		
12	0.2 M Magnesium chloride hexahydrate, 0.1 M HEPES sodium pH 7.5, 30% v/v 2-Propanol	P		
15	0.2 M Ammonium sulfate, 0.1 M Sodium cacodylate trihydrate pH 6.5, 30% w/v Polyethylene glycol 8,000			PH
16	0.1 M HEPES sodium pH 7.5, 1.5 M Lithium sulfate monohydrate		C	
17	0.2 M Lithium sulfate monohydrate, 0.1 M TRIS hydrochloride pH 8.5, 30% w/v Polyethylene glycol 4,000			PH
18	0.2 M Magnesium acetate tetrahydrate, 0.1 M Sodium cacodylate trihydrate pH 6.5, 20% w/v Polyethylene glycol 8,000			PH
20	0.2 M Ammonium sulfate, 0.1 M Sodium acetate trihydrate pH 4.6, 25% w/v Polyethylene glycol 4,000	P		
22	0.2 M Sodium acetate trihydrate, 0.1 M TRIS hydrochloride pH 8.5, 30% w/v Polyethylene glycol 4,000	P		
24	0.2 M Calcium chloride dihydrate, 0.1 M Sodium acetate trihydrate pH 4.6, 20% v/v 2-Propanol			PH
26	0.2 M Ammonium acetate, 0.1 M Sodium citrate tribasic dihydrate pH 5.6, 30% v/v (+/-)-2-Methyl-2,4-pentanediol	P		
27	0.2 M Sodium citrate tribasic dihydrate, 0.1 M HEPES sodium pH 7.5, 20% v/v 2-Propanol	P		
28	0.2 M Sodium acetate trihydrate, 0.1 M Sodium cacodylate trihydrate pH 6.5, 30% w/v Polyethylene glycol 8,000	P		
30	0.2 M Ammonium sulfate, 30% w/v Polyethylene glycol 8,000	P		
31	0.2 M Ammonium sulfate, 30% w/v Polyethylene glycol 4,000		C	
32	2.0 M Ammonium sulfate	P		
33	4.0 M Sodium formate		C	
34	0.1 M Sodium acetate trihydrate pH 4.6, 2.0 M Sodium formate			PH
35	0.1 M HEPES sodium pH 7.5, 0.8 M Sodium phosphate monobasic monohydrate, 0.8 M Potassium phosphate monobasic	P		
37	0.1 M Sodium acetate trihydrate pH 4.6, 8% w/v Polyethylene glycol 4,000		C	
40	0.1 M Sodium citrate tribasic dihydrate pH 5.6, 20% v/v 2-Propanol, 20% w/v Polyethylene glycol 4,000	P		
41	0.1 M HEPES sodium pH 7.5, 10% v/v 2-Propanol, 20% w/v Polyethylene glycol 4,000	P		
42	0.05 M Potassium phosphate monobasic, 20% w/v Polyethylene glycol 8,000	P		
43	30% w/v Polyethylene glycol 1,500	P		
44	0.2 M Magnesium formate dihydrate	P		
45	0.2 M Zinc acetate dihydrate, 0.1 M Sodium cacodylate trihydrate pH 6.5, 18% w/v Polyethylene glycol 8,000		C	
46	0.2 M Calcium acetate hydrate, 0.1 M Sodium cacodylate trihydrate pH 6.5 , 18% w/v Polyethylene glycol 8,000	P		
47	0.1 M Sodium acetate trihydrate pH 4.6, 2.0 M Ammonium sulfate	P		
48	0.1 M TRIS hydrochloride pH 8.5, 2.0 M Ammonium phosphate monobasic	P		
49	1.0 M Lithium sulfate monohydrate, 2% w/v Polyethylene glycol 8,000	P		
50	0.5 M Lithium sulfate monohydrate, 15% w/v Polyethylene glycol 8,000	P		
	Crystal Screen 2 ™ - HR2-112 Sample concentration: 8.8 mg.ml Drop formula: (0.8 µl samle + 0.8 µl reservoir) against 500 µl resevoir	Interpretation		
1	2.0 M Sodium chloride, 10% w/v Polyethylene glycol 6,000	P		
2	0.5 M Sodium chloride, 0.01 M Magnesium chloride hexahydrate, 0.01 M Hexadecyltrimethylammonium bromide	P		
3	25% v/v Ethylene glycol		C	
4	35% v/v 1,4-Dioxane	P		
5	2.0 M Ammonium sulfate, 5% v/v 2-Propanol	P		
7	10% w/v Polyethylene glycol 1,000, 10% w/v Polyethylene glycol 8,000	P		
8	1.5 M Sodium chloride, 10% v/v Ethanol	P		
9	0.1 M Sodium acetate trihydrate pH 4.6, 2.0 M Sodium chloride	P		
10	0.2 M Sodium chloride, 0.1 M Sodium acetate trihydrate pH 4.6, 30% v/v (+/-)-2-Methyl-2,4-pentanediol	P		

Another screening was set up using the conditions derived from successful NMT crystallization in other organisms. There were totally seven conditions that had been tried (Table 2). Different concentrations of the protein have been also taken into account, and different drop volume formulas have been considered. After 2 weeks, there was still no hit observed.

Table 2: Crystallization screening with conditions from literature on successful NMT crystallization. Interpretation: P: precipitate, C: clear, PH: phase separation

	Sample concentration: 18 mg.ml Drop formula: (1 µl samle + 1 µl reservoir) against 500 µl resevoir	Interpretation
1	20 mM HEPES pH 7.1, 2.6 M ammonium sulfate	C
2	9-11% (w/v) polyethylene glycol 4000, 50 mM zinc acetate, 100 mM sodium cacodylate pH 6.8, 21.5 % (v/v) glycerol	P
3	15-18% (w/v) polyethylene glycol 3350, 0.2 M lithium sulfate, 50 mM HEPES pH 7.5	C
4	100 mM Tris-HCl pH 6.8-7.2, 10% (w/v) polyethylene glycol 4000, 15% (v/v) glycerol	P
5	0.6 M lithium chloride, 20% (w/v) polyethylene glycol 6000, 1,4-pentanediol in 0.5 M sodium citrate pH 6.0	P
6	20% (w/v) polyethylene glycol 1500, 0.2 M NaCl, 0.1 M sodium cacodylate pH 5.6	P
7	19% (w/v) polyethylene glycol 3350, 0.2 M diamonium hydrogen citrate pH 5.7	PH
	Sample concentration: 18 mg.ml Drop formula: (2 µl samle + 2 µl reservoir) against 500 µl resevoir	Interpretation
1	20 mM HEPES pH 7.1, 2.6 M ammonium sulfate	C
2	9-11% (w/v) polyethylene glycol 4000, 50 mM zinc acetate, 100 mM sodium cacodylate pH 6.8, 21.5 % (v/v) glycerol	P
3	15-18% (w/v) polyethylene glycol 3350, 0.2 M lithium sulfate, 50 mM HEPES pH 7.5	C
4	100 mM Tris-HCl pH 6.8-7.2, 10% (w/v) polyethylene glycol 4000, 15% (v/v) glycerol	P
5	2.0 M Ammonium sulfate, 5% v/v 2-Propanol	P
6	10% w/v Polyethylene glycol 1,000, 10% w/v Polyethylene glycol 8,000	P
7	19% (w/v) polyethylene glycol 3350, 0.2 M diamonium hydrogen citrate pH 5.7	P
	Sample concentration: 9 mg.ml Drop formula: (1 µl samle + 1 µl reservoir) against 500 µl resevoir	Interpretation
1	20 mM HEPES pH 7.1, 2.6 M ammonium sulfate	C
2	9-11% (w/v) polyethylene glycol 4000, 50 mM zinc acetate, 100 mM sodium cacodylate pH 6.8, 21.5 % (v/v) glycerol	P
3	15-18% (w/v) polyethylene glycol 3350, 0.2 M lithium sulfate, 50 mM HEPES pH 7.5	C
4	100 mM Tris-HCl pH 6.8-7.2, 10% (w/v) polyethylene glycol 4000, 15% (v/v) glycerol	P
5	2.0 M Ammonium sulfate, 5% v/v 2-Propanol	P
6	10% w/v Polyethylene glycol 1,000, 10% w/v Polyethylene glycol 8,000	P
7	19% (w/v) polyethylene glycol 3350, 0.2 M diamonium hydrogen citrate pH 5.7	PH
	Sample concentration: 9 mg.ml Drop formula: (1 µl samle + 1 µl reservoir) against 500 µl resevoir	Interpretation
1	20 mM HEPES pH 7.1, 2.6 M ammonium sulfate	C
2	9-11% (w/v) polyethylene glycol 4000, 50 mM zinc acetate, 100 mM sodium cacodylate pH 6.8, 21.5 % (v/v) glycerol	P
3	15-18% (w/v) polyethylene glycol 3350, 0.2 M lithium sulfate, 50 mM HEPES pH 7.5	P
4	100 mM Tris-HCl pH 6.8-7.2, 10% (w/v) polyethylene glycol 4000, 15% (v/v) glycerol	P
5	2.0 M Ammonium sulfate, 5% v/v 2-Propanol	P
6	10% w/v Polyethylene glycol 1,000, 10% w/v Polyethylene glycol 8,000	P
7	19% (w/v) polyethylene glycol 3350, 0.2 M diamonium hydrogen citrate pH 5.7	P

Part 4: Discussion

4.1. *Pf*NMT expression and purification

4.1.1 Expression

The expression level of *Pf*NMT was improved in comparison to the previous attempt to express this protein in *E.coli* (Gunaratne, Sajid et al. 2000), in which only 12 μg of *Pf*NMT was yielded from one liter of culture. The problem of expression was the skewed codon usage in a heterologous system like *E. coli*. This could be partly overcome by using the *E. coli* BL21(*DE3*)-RIL strain since the RIL construct encoded tRNAs with rare codons, which were not preferred by *E. coli*. In addition, there was no protein in the cell debris after sonication, i.e *Pf*NMT was present in soluble form in the cell lysate and did not form inclusion bodies. The overall yield, however, was still low, approximately 0.1 $mg.l^{-1}$ of culture.

4.1.2 Purification

Using continuous gradient of imidazole to elute His-*Pf*NMT did not give good separation; and thus the step-wise elution could help remove the non-specific binding proteins more effectively. Including 40 mM imidazole in binding buffer gave even more efficient purification because of shorter washing time.

The capacity of the Nickel-Sepharose column Fast Flow 6 (10 ml) was probably insufficient for the load of lysate from 10 liters of culture, since there was about one-fourth of the protein present in the flowthrough (Figure 16F).

Imidazole might disrupt the stability of the protein since precipitation was observed when the eluent from Nickel-Sepharose column was freezed and thawed. It is thus strongly suggested to do a desalting step after IMAC to keep the protein in good state.

Multiple bands, which were supposed to be His-*Pf*NMT and its cleavage products, appeared after SEC on Superdex 75 column. This problem might be due to proteolysis by residual proteases remaining on the column. Nonetheless, the Superdex 200 could give better resolution of His-*Pf*NMT from the proteins whose molecular weights were higher than 75 kDa, although its retention time would be longer than using Superdex 75 column (80 min versus 58 min).

In IEX step, there were at least four overlapping peaks eluted using a gradient of NaCl from 0.1 to 1 M. The result of SDS-PAGE (Figure 16D) proved the presence of His-*Pf*NMT in all four fractions, indicating that the proteins were different from each other in terms of binding affinity to the Mono S column, and the structural characteristics as well. This inhomogeneity might result in low yield of *Pf*NMT expression. The major His-*Pf*NMT species was the one eluted by solution containing 0.37 M NaCl using step-wise concentration gradient.

The final SEC step is necessary to exclude any aggregated proteins. Because SEC requires a very small column like 1 or 0.5 ml, concentrating prior to loading must be

done; and this occasionally causes loss of protein. Therefore, SEC should be avoided as much as possible. In conclusion, the 4-step purification comprising IMAC-Desalting-IEX-SEC seems to be ideal for 6xHis-*Pf*NMT in the range of this study.

4.1.3 Final PfNMT purity

Good purity is crucial for crystallization. Here a protein with molecular weight of about 25 kDa was still present at considerable amount in the purified His-*Pfi*NMT. A corresponding protein had been reported in previous study in which His-*Pf*NMT was expressed and purified from *E. coli*. The protein was identified, and confirmed by peptide mass fingerprinting, as CAP-DNA recognition protein (Bowyer, Gunaratne et al. 2007), or Crp (NCBI accession number **GI:16131236**, UniProtKB/Swiss-Prot accession number **P0ACJ8**).

4.2. *Pf*NMT activity, pH and temperature stability

4.2.1 PfNMT activity

The K_m values for the synthetic peptide substrate (GSCYSRKN) were identified at sub-millimolar level for both His-PfNMT and PfNMT without 6xHis-tag. These indicated a low affinity of the peptide to the enzyme. The peptide was derived from eight N-terminal residues of *P. falciparum* adenylate kinase 2 (*Pf*AK2), which has been identified as a putative substrate for *Pf*NMT (Rahlfs, Koncarevic et al. 2009). The full-length *Pf*AK2 showed strong interaction with *Pf*NMT (through gel filtration and MALDI-MS analysis) when they were co-expressed in *E. coli* with the supplement of myristate (Rahlfs, Koncarevic et al. 2009).

Previous studies on His-*Pf*NMT (Bowyer, Gunaratne et al. 2007) reported SPA (Scintillation Proximity Assay), in which the transfer of radio-labeled myristoyl ([^{3}H]myristate) moiety to the peptide was detected. In principle, the peptide was biotinylated and thus could be bound to streptavidin-coated scintillant beads. Various peptides were assayed by SPA and exhibited different specificity to the enzyme (Table 3). It is obvious that one residue difference in the peptide length can make a significant K_m difference (almost 6 times). The sequences of these peptides, as well as the *Pf*AK2 derivative, meet the requirements of a putative N-myristoylated target by *S. cerevisiae* Nmt1p (Farazi, Waksman et al. 2001).

Table 3: Different peptides determined as substrate for *Pf*NMT or not (Bowyer, Gunaratne et al. 2007)

Peptide sequence	Name	Number of residues	K m (μM)
GLYVSRLFNRLFQKK(biotin)-NH2	ARFlong	15	1.2+-0.4
GLYVSRLFNRLFQK(biotin)-NH2	ARFshort	14	7.1+-1.0
GSQGSKPVDTSDVK(biotin)-NH2	*Pf*EMP	15	Not a substrate
ALYVSRLFNRLFQKK(biotin)-NH2	AlaARFlong	15	Not a substrate
ALYVSRLFNRLFQK(biotin)-NH2	AlaARFshort	14	Not a substrate

ARF: ADP-ribosylation factors, *Pf*EMP: *P. falciparum* erythrocyte membrane protein

SPA has been reported to be faster, more sensitive and high-throughput than using DTNB (or Ellman reagent). In a certain case like this study, the peptide substrate contains a sulfhydryl group in Cystein side-chain, which interferes much on the quantification of thiol groups by spectrophotometric measurement, especially when the peptide concentration exceeds that of the released thiols.

4.2.2 pH and temperature stability

*Pf*NMT experimentally showed highest activity at pH 6.5, which was a bit weird in comparison to other NMT homologs (Table 4), most of which have the pH optimum at 7.4 (closed to physiological pH). The putative *Pf*AK2 was supposed to be localized and function in the apicoplast, a plastid-like organ in *P. falciparum* (Rahlfs, Koncarevic et al. 2009). Therefore, N-myristoylation of *Pf*AK2 would likely occur inside this compartment. More interestingly, the *de novo* fatty acid synthesis by type II FAS has been known to take place in apicoplast (Waller, Ralph et al. 2003), and mostly that the myristoyl-CoA which is necessary for *Pf*NMT activity is possibly synthesized here. There are still limited data on functions of this plastid-like organ in *P. falciparum*. If the pH inside apicolplast stroma were slightly acidic, it would probably makes senses that the ideal pH for N-myristoylation by *Pf*NMT is at pH less than 7.0. In addition, the localization of *Pf*NMT should be studied to confirm its pH optimum.

Table 4: pH optimum, pH stability and temperature optimum of N-myristoyltransferase in some species

	pH optimum	pH stability range	Temperature optimum	References
Saccaromyces cerevisiae	7.4	7.0 - 9.0	30	(Wagner and Retey 1991)
Arabidopsis thaliana	7.8	5.5 - 8.5	-	(Qi, Rajala et al. 2000)
Bos taurus	7.5	-	37	(King and Sharma 1993); (Glover and Felsted 1995)
Mus musculus	7.8	-	30	(Paige, Chafin et al. 1989)
Homo sapiens	7.4	-	30	(Pasha, Dimmock et al. 2002)

"-": not yet determined

The temperature at which *Pf*NMT is active the most was determined as 37^0C. This indicates that the enzyme is more likely active at asexual blood-stage inside human host than at the zygote or the sporozoite stage in mosquitoes. This result is supported by a study on gene expression in *P. falciparum* in which the single *NMT* gene was identified to be expressed only at blood-stage. Other NMTs in different species have optimal temperature at 30^0C or 37^0C (Table 4).

4.3. Isothermal titration calorimetry

There was no binding of the octapeptide to *Pf*NMT in the absence of myristoyl-CoA, and this seems to agree with the knowledge on NMT substrate recognition in general. However, the experiment on *Pf*NMT:myristoyl-CoA binding gained no positive result. In fact, NMT has been known to have high affinity to myristoyl-CoA. A binding study of *S. cerevisiae* Nmt1p and different myristoyl-CoA analogs were carried out, and all have the K_d of nanomolar level (Table 5) (Bhatnagar, Schall et al. 1997).

In order to investigate the binding site of the peptide, a non-hydrolyzable myristoyl-CoA analog and a peptide-mimetics should be utilized. For Nmt1p, *S*-(2-oxo)pentadecylCoA and a peptide derived from *Sc*Arf2p were used.

Table 5: Thermodynamics parameters in binding study of different substrates including myristoyl-CoA and its analogs to *S. cerevisiae* Nmt1p; and the peptide mimetics to Nmt1p:myristoyl-CoA complex (Bhatnagar, Schall et al. 1997)

	K_d (nM)	ΔH (kcal/mol)	TΔS (kcal/mol)
myristoylCoA	15	-24.8	-14.1
S-(2-oxo)pentadecylCoA(1)	3	-25.8	-14.1
2-hydroxymyristoylCoA(2)	33	-23.6	-13.3
myristoyl-3'-dephosphoCoA(3)	124	-17.5	-8.0
SC-58272(4) to Nmt1p:myristoyl-CoA	29	-14.0	-13.7

(1): non-hydrolyzable myristoyl-CoA analog with a methylene group between CoA sulfur and fatty acid carbonyl carbonyl; (2) an inhibitor of Nmt1p; (3) myristoyl-CoA analog without 3'-phosphate group; (4) peptide mimetics inhibitor of Nmt1p, derived from ScArf2p

4.4. Crystallization

Unfortunately, no hit was obtained from crystallization trial. This might be because of several reasons such as not very good purity of *Pf*NMT, inappropriate concentration, not suitable reservoirs, insufficient screening conditions, or even handling in crystallization set up.

48 out of 55 tried conditions were from Hampton Crystal Screen Kits, and 7 remaining conditions were selected from successful crystallization of NMTs from other species like *S. cerevisiae*, *C. albicans*, *T. brucei*, *L. donovani*, *L. major* and human. The concentration of NMTs required in each successful case was much varying.

Part 5: Materials and Methods

5.1. Chemical and reagents

All chemicals and reagents used in this study were obtained from commercial sources: Merck, GE Healthcare, Sigma-Aldrich, Novagen, Fluka, Stratagene.

5.2. Media

The media used for bacteria culture were LB (Luria-Bertani broth) and 2xYT, which is optimized for the growth, maintenance and propagation of *E. coli*. The enriched 2xYT medium allows the bacteria to growth faster, and expressed the recombinant protein in more quantity since it contains it contains more amino acids, precursors of nucleotides, vitamins and other metabolisms.

One liter LB is composed of 10 g tryptone, 5 g yeast extract and 10 g NaCl dissolved in distilled water. LB-agar medium is LB with 1% (w/v) agar. One liter 2xYT contains 16 g tryptone, 10 g yeast extract and 5 g NaCl dissolved in distilled water. All media were sterilized by autoclaving and stored at 37^0C (one day before use) or at 4^0C (long term storage). One liter of TB contains 12 g tryptone, 24 g yeast extract and 40 mM phosphate buffer pH 7.0.

Antibiotic stocks: two antibiotics, kanamycine (sulfate salt) and chloramphenicol were used in this study. They were prepared at the concentrations of 25 and 34 $mg.ml^{-1}$ in distilled water and ethanol absolute as stock solutions, respectively. The suggested working concentration of each antibiotic was 1:1000 and 1:700 dilution of the stock, respectively.

5.3. Host cells and Vectors

Escherichia coli BL21(*DE3*) C41 strain was used as competent cells for DNA transformation. The DE3 recombinant phage harboring the *T7 RNA polymerase* gene that can drive the expression at high level of the genes cloned under the control of T7 promoter.

The pET-28 plasmid contains a T7 promotor, which can be induced by IPTG for over-expression of the recombinant protein. The vector also carries a kanamycine-resistant gene, which can be used as a selective marker.

The RIL construct was used in co-transformation to overcome the condon usage bias of the *E.coli* host cells. The construct encodes the tRNAs that are compatible with the rare codons in cloned genes, and additionally the chloramphenicol-resistant gene for selection.

All plasmids were stored at -20^0C. *E.coli* competent cells were stored at -80^0C in glycerol stock.

5.4. Methods and Equipments

5.4.1 Expression of 6xHis-tagged PfNMT

Plasmodium falciparum NMT (*Pf*NMT) ORF was previously cloned between the restriction sites of *Bam*HI and *Eco*RI of pET28 vector with a 6xHistidine tag and T7 tag at the N-terminus. The sequence of the cloned gene was already confirmed. A thrombin cleavage site was encoded between the two tags so that the His-tag could be cleaved off from the protein later on.

The pET28-*Pf*NMT construct was transformed into *E. coli* BL21(*DE3*)-RIL strain C41 by electroporation using E. coli Pulser apparatus (BIO-RAD). The transformed cells were selected on a LB-agar plate supplied with 20 $\mu g.ml^{-1}$ kanamycine and 19 $\mu g.ml^{-1}$ chloramphenicol (here the practical working concentration was 20% less than suggestions to ensure the bacteria grow well in the presence of two antibiotics). The plate was kept at 37^0C overnight.

One single colony was picked up from the plate and was inoculated to 50 ml of 2xYT medium in a 250 ml conical flask, supplemented with kanamycin and chloramphenicol at the same concentration as above. This primary culture was kept at 37^0C with vigorous shaking (200 rpm) overnight.

To make secondary culture for *Pf*NMT production, 10 ml of the primary culture was inoculated into 1 L of 2xYT medium supplied with kanamycin and chloramphenicol (practical concentration was 40% less than suggestions for faster growth) in 2 L conical flask. The culture was kept at 37^0C with vigorous shaking, and the absorbance at 600 nm (OD_{600}) was recorded every 30 minutes. When the OD_{600} was in the range of 0.5-0.6, the culture was induced with 300 µl of 1 M IPTG (final concentration was 0.3 mM), and then was kept at 28^0C on the shaker (rpm)

After 6 hours, the culture was centrifuged at 6000 rpm in 20 min at 4^0C, the cells were then re-suspended in lysis buffer (Table 1), and the ratio was 70 ml lysis buffer for the batch of 5 litter of secondary culture. Cells were resuspended at 4^0C in 30 minutes and then lysed at 37^0C in 20 minutes with mild shaking. The lysed cells were disrupeted using sonicator (30% amplitude in 2 min for each 50 ml lysate, with 1 min rest on ice in between). The suspension was centrifuged at 20,000 rpm in 40 min at 4^0C, and the supernatant was collected. *Pf*NMT was purified from the lysate by liquid chromatography.

5.4.2 Purification of recombinant PfNMT

A multi-step strategy was applied for *Pf*NMT purification including affinity, ion exchange, and size exclusion chromatography on AKTA Purifier or AKTA Explorer FPLC platform.

Immobilized metal affinity chromatography (IMAC)

The lysate was loaded on Nickel-Sepharose Fast Flow column (GE Healthcare). The column was initially equilibrated with binding buffer (Table 1) for ~5 column volume

or until the base line was stable. The flow-rate was controlled at 5 ml.min^{-1}. The unbound proteins were collected as "flowthrough". The column was continually washed with several column volume of binding buffer until the 280 nm-absorbance curve came to 0.

*Pf*NMT was eluted with elution buffer (Table 1). The eluent was buffer-exchanged to 25 mM Tris pH 7.0, 0.1 M NaCl using HiPrep™ 26/10 Desalting Column (GE Healthcare), and then concentrated to 1 ml using Vivaspin^{TM} 10,000 MWCO centricon (Cole-Parmer).

Size exclusion chromatography

The HiLoad 16/60 Superdex 200 (SD200) column (GE Healthcare) was equilibrated with buffer containing 25 mM Tris-HCl pH 7.0, 0.1 M NaCl (1 column volume, or 120 ml) at 1 ml.min^{-1} flow-rate. The concentrated sample was injected into the column and the buffer flowed through at the same speed. One-ml-sized fractions were collected. Peak fractions were analyzed by SDS-PAGE and fractions containing NMT were pooled.

Cation exchange chromatography

The cation exchange Mono-S column (GE Healthcare) was first equilibrated with binding buffer (Table 1). The pooled SD200 sample was loaded on the column. The flow-rate was kept as low as 1 ml.min^{-1}, and the pressure was controlled under 4 MPa. The column was washed with binding buffer until the 280 nm absorbance curve came to 0 or remained stable. The protein was then eluted using a continuous gradient of elution buffer (Table 1) from 0% to 100%, and was fractioned in 0.33 ml each. The purity of *Pf*NMT was confirmed by SDS-PAGE.

Thrombin digestion

The 6xHis-tag of purified *Pf*NMT was cleaved off using Thrombin Cleavage Capture Kit (Novagen). One unit of thrombin (equivalently to 1 µl) was required for 1 mg of target protein. The digestion was done in 1X cleavage buffer. The mixture was incubated at room temperature. One µl from the mixture was removed after 0, 4, 8, 12 hours and was run on SDS-PAGE gel to monitor the digestion.

5.4.3 Western blotting

The protein samples were separated by Sodium-dodecyl sulfate polyacrylamide gel electrophoresis (SDS-PAGE) (Appendix). The detailed protocol of Western blot is given in Appendix1.

Blotting

The proteins on the gel were electro-blotted to a nitrocellulose membrane (Amersham^{TM}-Hybond^{TM} ECL, GE Healthcare) at 30 volts overnight. When the blotting was done, the membrane was treated with signaling enhancer reagents from Qentix^{TM}Western Blot Siganl Enhancer (Thermo Scientific).

Blocking

The blotted membrane incubated with blocking buffer, which was composed of 5% blotting-grade non-fat dry milk (BIO-RAD) in 1x PBS buffer for 4 hours with mild shaking to block all non-specific binding to the membrane.

Antibody incubation

The anti-N-terminal polyhistidine antibody was used to detect the presence of His-*Pf*NMT. The antibody was prepared in BBT (blocking buffer with 0.1 % Tween) at the concentration of . The blot was washed with PBST (PBS buffer with 0.1% Tween 20) and then was incubated with the antibody solution for 1 hour.

Detecting

The blot was washed thoroughly with PBST to remove the trace of antibody. It was then incubated with Detection Reagents (Thermo Scientific) and exposed to CL-XPosure^{TM} film (Thermo Scientific) in a dark room. The film was submerged in developer and fixation solutions for visualizing the detected proteins.

5.4.4 Protein concentration determination

The protein concentration was determined using Bradford assay. A series of BSA concentration standards was prepared: 0.1, 0.15 and 0.2 mg.ml^{-1} in distilled water. One ml of Bradford reagent (Sigma) was added to 15 µl of BSA solution. The absorbance at 595 nm (OD_{595}) was recorded and blanked against distilled water using Shimadzu Bio-Mini 1240 Spectrophotometer (Spectrum Chemicals & Laboratory Products), then was plotted versus the concentrations of BSA. The protein sample was diluted to appropriate concentration and assayed in the same way and the concentration was calculated from the standard curve. The measurement was carried out in duplex.

For fast and easy determination, NanoDrop ND-1000 Spectrophotometer (Thermo scientific) was used since it required a volume as small as 1 µl of the sample without cuvettes or any dilutions.

5.4.5 Enzymatic activity assay

The specific activity of *Pf*NMT, given in '(nmol of thiol).mg^{-1}.min^{-1}, was measured by determining the amount of thiol group produced upon the release of CoA, according to Wu, Tao et. al (2007). Synthetic myristoyl-CoA and octapeptide (GSCYSRKN) substrate were used as substrates. Both His-tagged *Pf*NMT and *Pf*NMT without tag were assayed. The experiment was done at least in two replicates. Some kinetic parameters for the myristoylation by *Pf*NMT were determined as described below.

V_{max} and K_m

Each enzymatic reaction was carried-out in a 1.5 ml test tube. The mixture contained 5 μM *Pf*NMT (equivalent to ~13 μg), 0.16 mM MCoA and the peptide with a range of concentration (varying from 0.1 to 1 mM) in 0.1 M HEPES buffer pH 7 to make the final volume of 50 μl. The mixture was incubated at 37^0C for 1 hour. After that, 25 μl of 10 mM 5,5'-dithiobis(2-nitrobenzoic acid) (DTNB) in 0.1 M Tris-HCl pH 8.0 was added to stop the reaction, followed by the addition of 35 μl of 0.1 M Tris-HCl pH 8.0 and 390 μl distilled water. The absorbance at 412 nm (OD_{412}) of the mixture was measured using Shimadzu Bio-Mini 1240 Spectrophotometer (Spectrum Chemicals & Laboratory Products). A corresponding sample of each reaction without the enzyme was taken as control. A standard curved of OD_{412} versus the known concentrations of β-mercaptoethanol (through reaction with DTNB) was prepared to calculate the amount of thiol group released. The *V_{max} and K_m* values were calculated by fitting the data into the Michaelis-Menten equation with nonlinear regression using program.

Optimal pH and temperature

Similar assays were performed with fixed concentration of the peptide substrate (1 mM) in different pH and temperatures. The enzyme activity was determined in a pH range of 6-8; a series of buffer systems (Table 1) were used, and all reactions were done at 37^0C. Simultaneously, another set of reactions at pH 7.5 was carried out at 4 different temperatures: 20^0C, 25^0C, 37^0C and 45^0C. At the optimal conditions, which are ideal for the enzyme catalysis, the specific activity of *Pf*NMT is maximum.

5.4.6 Isothermal titration calorimetry

The concentration of purified *Pf*NMT was 2 μM in 25 mM Tris-HCl pH 7.0, 0.1 M NaCl. Myristoyl-CoA and the octapeptide substrate were prepared in the same buffer with the concentration of 40 μM. Calorimetric titrations were performed using VP-ITC Isothermal Titration calorimeter (MicroCal, GE Healthcare). Data from each titration were collected in MicroCal Origin software. Baseline thermal current subtraction and peak integration limits were adjusted within Origin. Titrations were carried out at 37^0C.

5.4.7 Crystallization trial

Crystallization was set up using sitting-drop vapor diffusion method. Various conditions were screened using *Crystallization Screen* kits from Hampton Research. The purified *Pf*NMT solution was concentrated to approximately 10 $mg.ml^{-1}$ using Vivaspin^{TM} MWCO 10,000. Typically a drop of 1 µl concentrated protein was mixed with 1 µl reservoir, and the mixture was diffused against 500 µl reservoir. Different protein concentration and drop formulas were also examined. The crystallization plates were incubated at 20^0C.

Table 6: List of buffers used in the purification and enzymatic assay of *Pf*NMT

Buffers	Components
Lysis	20 mM Tris pH 7.0, 0.1 M NaCl, 0.1 % lysozyme (w/w), 1 EDTA-free protease inhibitors tablet (Roche)
IMAC binding buffer	20 mM phosphate pH 7.0, 0.5 M NaCl, 40 mM imidazole
IMAC elution buffer	20 mM phosphate pH 7.0, 0.5 M NaCl, 250 mM imidazole
Size exclusion chromatography buffer	25 mM Tris-HCl pH 7.0, 0.1 M NaCl
IEX binding buffer	25 mM Tris-HCl pH 7.0, 0.1 M NaCl
IEX elution buffer	25 mM Tris-HCl pH 7.0, 1 M NaCl
Enzymatic assay buffers	0.1 M MES buffer pH 6.0
	0.1 M MES buffer pH 6.5
	0.1 M HEPES buffer pH 7.5
	0.1 M HEPES buffer pH 7.5
	0.1 M Tris-HCl buffer pH 8.0
	0.1 M Tris-HCl buffer pH 8.5

References

Bhatnagar, R. S., O. F. Schall, et al. (1997). "Titration calorimetric analysis of AcylCoA recognition by myristoylCoA:protein N-myristoyltransferase." Biochemistry **36**(22): 6700-6708.

Bhatnagar, R. S., K. Futterer, et al. (1998). "Structure of N-myristoyltransferase with bound myristoylCoA and peptide substrate analogs." Nat Struct Biol **5**(12): 1091-1097.

Bhatnagar, R. S., K. Futterer, et al. (1999). "The structure of myristoyl-CoA:protein N-myristoyltransferase." Biochim Biophys Acta **1441**(2-3): 162-172.

Boutin, J. A. (1997). "Myristoylation." Cell Signal **9**(1): 15-35.

Bowyer, P. W., R. S. Gunaratne, et al. (2007). "Molecules incorporating a benzothiazole core scaffold inhibit the N-myristoyltransferase of Plasmodium falciparum." Biochem J **408**(2): 173-180.

Brannigan, J. A., B. A. Smith, et al. (2010). "N-myristoyltransferase from Leishmania donovani: structural and functional characterisation of a potential drug target for visceral leishmaniasis." J Mol Biol **396**(4): 985-999.

Devadas, B., S. K. Freeman, et al. (1997). "Design and synthesis of novel imidazole-substituted dipeptide amides as potent and selective inhibitors of Candida albicans myristoylCoA:protein N-myristoyltransferase and identification of related tripeptide inhibitors with mechanism-based antifungal activity." J Med Chem **40**(16): 2609-2625.

Duronio, R. J., D. A. Towler, et al. (1989). "Disruption of the yeast N-myristoyl transferase gene causes recessive lethality." Science **243**(4892): 796-800.

Farazi, T. A., G. Waksman, et al. (2001). "The biology and enzymology of protein N-myristoylation." J Biol Chem **276**(43): 39501-39504.

Frearson, J. A., S. Brand, et al. (2010). "N-myristoyltransferase inhibitors as new leads to treat sleeping sickness." Nature **464**(7289): 728-732.

Glover, C. J., M. R. Tellez, et al. (1991). "Synthesis and characterization of inhibitors of myristoyl-CoA:protein N-myristoyltransferase." Biochem Pharmacol **41**(6-7): 1067-1074.

Glover, C. J. and R. L. Felsted (1995). "Identification and characterization of multiple forms of bovine brain N-myristoyltransferase." J Biol Chem **270**(39): 23226-23233.

Glover, C. J., K. D. Hartman, et al. (1997). "Human N-myristoyltransferase amino-terminal domain involved in targeting the enzyme to the ribosomal subcellular fraction." J Biol Chem **272**(45): 28680-28689.

Goodman, L. S., A. Gilman, et al. (2008). Goodman & Gilman's manual of pharmacology and therapeutics. New York, McGraw-Hill Medical.

Gunaratne, R. S., M. Sajid, et al. (2000). "Characterization of N-myristoyltransferase from Plasmodium falciparum." Biochem J **348 Pt 2**: 459-463.

King, M. J. and R. K. Sharma (1993). "Identification, purification and characterization of a membrane-associated N-myristoyltransferase inhibitor protein from bovine brain." Biochem J **291 (Pt 2)**: 635-639.

Marcus, B. A. (2009). Malaria. New York, NY, Chelsea House.

Maurer-Stroh, S. and F. Eisenhaber (2004). "Myristoylation of viral and bacterial proteins." Trends Microbiol **12**(4): 178-185.

Ntwasa, M., S. Aapies, et al. (2001). "Drosophila embryos lacking N-myristoyltransferase have multiple developmental defects." Exp Cell Res **262**(2): 134-144.

Paige, L. A., D. R. Chafin, et al. (1989). "Detection of myristoyl CoA:protein N-myristoyltransferase activity by ion-exchange chromatography." Anal Biochem **181**(2): 254-258.

Panethymitaki, C., P. W. Bowyer, et al. (2006). "Characterization and selective inhibition of myristoyl-CoA:protein N-myristoyltransferase from Trypanosoma brucei and Leishmania major." Biochem J **396**(2): 277-285.

Pasha, M. K., J. R. Dimmock, et al. (2002). "Enhanced activity of human N-myristoyltransferase by dimethyl sulfoxide and related solvents in the presence of serine/threonine-containing peptide substrates." Biochem Pharmacol **64**(10): 1461-1467.

Perkins, S. L. and C. C. Austin (2009). "Four new species of *Plasmodium* from New Guinea lizards: integrating morphology and molecules." J Parasitol **95**(2): 424-433.

Price, H. P., M. R. Menon, et al. (2003). "Myristoyl-CoA:protein N-myristoyltransferase, an essential enzyme and potential drug target in kinetoplastid parasites." J Biol Chem **278**(9): 7206-7214.

Qi, Q., R. V. Rajala, et al. (2000). "Molecular cloning, genomic organization, and biochemical characterization of myristoyl-CoA:protein N-myristoyltransferase from Arabidopsis thaliana." J Biol Chem **275**(13): 9673-9683.

Rahlfs, S., S. Koncarevic, et al. (2009). "Myristoylated adenylate kinase-2 of Plasmodium falciparum forms a heterodimer with myristoyltransferase." Mol Biochem Parasitol **163**(2): 77-84.

Rudnick, D. A., C. A. McWherter, et al. (1991). "Kinetic and structural evidence for a sequential ordered Bi Bi mechanism of catalysis by Saccharomyces cerevisiae myristoyl-CoA:protein N-myristoyltransferase." J Biol Chem **266**(15): 9732-9739.

Sheng, C., H. Ji, et al. (2009). "Homology modeling and molecular dynamics simulation of N-myristoyltransferase from protozoan parasites: active site characterization and insights into rational inhibitor design." J Comput Aided Mol Des **23**(6): 375-389.

Sogabe, S., M. Masubuchi, et al. (2002). "Crystal structures of Candida albicans N-myristoyltransferase with two distinct inhibitors." Chem Biol **9**(10): 1119-1128.

Stafford, W. H., R. W. Stockley, et al. (1996). "Isolation, expression and characterization of the gene for an ADP-ribosylation factor from the human malaria parasite, Plasmodium falciparum." Eur J Biochem **242**(1): 104-113.

Unicef. 2007. Malaria & Children: Progress in intervention coverage. The United Nations Children's Fund.

Wagner, A. P. and J. Retey (1991). "Synthesis of myristoyl-carba(dethia)-coenzyme A and S-(3-oxohexadecyl)-coenzyme A, two potent inhibitors of myristoyl-CoA:protein N-myristoyltransferase." Eur J Biochem **195**(3): 699-705.

Wahlgren, M. and Perlmann, P. 2005. Malaria: Molecular and Clinical Aspects. Hardwood Academic Publisher.

Waller, R. F., S. A. Ralph, et al. (2003). "A type II pathway for fatty acid biosynthesis presents drug targets in Plasmodium falciparum." Antimicrob Agents Chemother **47**(1): 297-301.

Weston, S. A., R. Camble, et al. (1998). "Crystal structure of the anti-fungal target N-myristoyl transferase." Nat Struct Biol **5**(3): 213-221.

Wilcox, C., J. S. Hu, et al. (1987). "Acylation of proteins with myristic acid occurs cotranslationally." Science **238**(4831): 1275-1278.

Wu, J., Y. Tao, et al. (2007). "Crystal structures of Saccharomyces cerevisiae N-myristoyltransferase with bound myristoyl-CoA and inhibitors reveal the functional roles of the N-terminal region." J Biol Chem **282**(30): 22185-22194.

Yang, S. H., A. Shrivastav, et al. (2005). "N-myristoyltransferase 1 is essential in early mouse development." J Biol Chem **280**(19): 18990-18995.

Appendix

Appendix 1: Detailed Western blot protocols

Buffer preparation

Table 7: Composition of SDS-PAGE gel

	Separating gel (4 gels)	Stacking gel (6 gels)
Ultra protogel (National Diagnostics, Atlanta)	10 ml	3 ml
1.5 M Tris-HCl pH 8.3	10 ml	-
0.5 M Tris-HCl pH 6.8	-	1.5 ml
SDS 20%	100 ml	75 ml
APS	200 ml	150 ml
TEMED	20 ml	7.5 ml
dH_2O	-	10.5 ml

- TGS buffer:

  25 mM TriS 3.03 g/l
  192 mM Glycine 14.4 g/l
  pH 8.3

- Sample buffer (Laemmli buffer):

  1 M Tris pH 6.8 2.4 ml
  SDS 0.8 g
  100% glycerol 4 ml
  0.01% Bromophenol blue 1.1 µl
  ß-mercaptoethanol 1 ml
  Distilled water 2.8 ml

- Protein transfer buffer (PTB):

  25 mM Tris 3.03 g/l
  192 mM Glycine 14.4 g/l
  20% Methanol 200 mL/l (only added before using)
  pH 8.3

- Phosphate buffer saline (PBS):

  137 mM NaCl 8 g/l
  2.7 mM KCl 0.2 g/l

10 mM Na_2HPO_4 1.44 g/l
2 mM NaH_2PO_4 0.24 g/l
pH 7.0

- PBST: PBS + 0.1% Tween 20
- Blocking buffer (BB): 5% non-fat dry milk in PBS
- BBT: BB + 0.1% Tween 20

SDS-PAGE

- SDS-PAGE gel casting (Table 7).
- Place gel in running chamber and fill with TGS Buffer.
- Heat samples at 95^0C for 10 minutes.
- Load 2 µl dual color marker (BIO-RAD).
- Load boiled samples (volume was estimated experimentally).
- Run at 150V constant until the blue bromophenol dye reaches the bottom of the gel.

Protein Transfer (Electro-blotting)

- Place gel and blotting pads in PTB
- Transfer gel to filter paper wetted in PTB.
- Assemble transfer apparatus in order: 2 x sponges, 3 x filter paper, gel, membrane , 3 x filter paper, 2 x sponges. Put the transfer cassette correctly: black face toward cathode and red/white face toward anode.
- Fill the chamber with PTB.
- Run 4 hours at 40V or overnight (at 4^0C) at 30V.

Blocking, washing, antibody incubation and detecting

- Incubate membrane in blocking solution for 5 hour at room temperature or at 4^0C overnight with shaking.
- Washing: with PBST, mild shaking
  3 times: 20 seconds
  1 time: 5 minutes
  1 time: 10 minutes
- Incubate primary antibody for 1 hour at room temperature.
- Remove antibody solution and wash membrane with PBST, mild shaking:
  3 times: 20 seconds
  1 time: 5 minutes

1 time: 10 minutes

- (Dark room) Mix 2 developing solutions and spread over the membrane.
- (Dark room) Expose membrane to X-ray film for 1 minute or less to achieve best results.

Appendix 2: Raw data of enzymatic assays

Michaelis-Meten modeling

Table 8: Data collected from enzymatic assay experiment when varying the concentration of the peptide substrate (AK2). The OD_{412} values were recorded in duplex and already blanked against the control (having same components as the sample except for the peptide)

His-*Pf*NMT: 0.92 µg protein per reaction

AK2 (mM)	OD_{412}			Released thiol		
	value 1	value 2	average	mM	nmol	nmol/mg protein/min
0	0	0	0	0	0	0
0.1	0.029	0.035	0.032	1.9231	0.9615	17.4192
0.2	0.084	0.082	0.083	5.8462	2.9231	52.9543
0.3	0.111	0.13	0.1205	8.7308	4.3654	79.0831
0.4	-	-	-	-	-	-
0.5	0.169	0.171	0.17	12.5385	6.2692	113.5730
0.6	-	-	-	-	-	-
0.7	0.197	0.189	0.193	14.3077	7.1538	129.5987
0.8	0.189	0.188	0.1885	13.9615	6.9808	126.4632
1	0.189	0.188	0.1885	13.9615	6.9808	126.4632

*Pf*NMT (no His-tag): 0.47 µg protein per reaction

AK2 (mM)	OD_{412}			Released thiol		
	value 1	value 2	average	mM	nmol	nmol/mg protein/min
0	0	0	0	0	0	0.0000
0.1	0.021	0.024	0.0225	1.1923	0.5962	21.1402
0.2	0.035	0.034	0.0345	2.1154	1.0577	37.5068
0.3	0.044	0.04	0.042	2.6923	1.3462	47.7360
0.4	0.067	0.06	0.0635	4.3462	2.1731	77.0595
0.6	0.071	0.086	0.0785	5.5000	2.7500	97.5177
0.7	0.085	0.085	0.085	6.0000	3.0000	106.3830
0.8	0.085	0.082	0.0835	5.8846	2.9423	104.3372
1	0.08	0.082	0.081	5.6923	2.8462	100.9274

pH and temperature optimum assay

Table 9: Data collected from pH and temperature (Temp.) optimum assay experiment. The OD_{412} values were recorded in duplex and already blanked against the control (having same components as the sample except for the peptide)

pH	OD412			Released thiol		
	value 1	value 2	average	mM	nmol	nmol/mg protein/min
6.0	0.676	0.678	0.677	51.53846	25.76923	85.8974
6.5	0.858	0.935	0.8965	68.42308	34.21154	114.0385
7.0	0.811	0.899	0.855	65.23077	32.61538	108.7179
7.5	0.695	0.774	0.7345	55.96154	27.98077	93.2692
8.0	0.692	0.694	0.693	52.76923	26.38462	87.9487
8.5	0.516	0.511	0.5135	38.96154	19.48077	64.9359

Temp. (^{0}C)	OD412			Released thiol		
	value 1	value 2	average	mM	nmol	nmol/mg protein/min
20	0.571	0.589	0.58	44.07692	22.03846	73.4615
25	0.653	0.687	0.67	51	25.5	85
37	0.836	0.893	0.8645	65.96154	32.98077	109.9359
45	0.752	0.696	0.724	55.15385	27.57692	91.9231